Unsupervised Domain Adaptation via Minimized Joint Error

Anonymous authors
Paper under double-blind review

Abstract

Unsupervised domain adaptation transfers knowledge from a learned source domain to a different target distribution, for which only few or no labeled data is available. Some researchers proposed upper bounds for the target error when transferring the knowledge, i.e., Ben-David et al. (2010) established a theory based on minimizing the source error and distance between marginal distributions simultaneously. However, in most works the joint error is usually ignored due to the intractability. In this paper, we argue that the joint error is essential for the domain adaptation problem, in particular if the samples from different classes in source/target are closely aligned when matching the marginal distributions due to a large domain gap. To tackle this problem, we propose a novel objective that relates to an upper bound of the joint error. Moreover, we adopt a source/pseudo-target labels induced hypothesis space that can reduce the searching space to further tighten up this bound. For the dissimilarity measurement between hypotheses, we propose a novel cross margin discrepancy to alleviate the instability during adversarial learning. In addition, we present extensive empirical evidence that shows that our proposal boosts the performance in image classification accuracy on standard domain adaptation benchmarks.

1 Introduction

The advent of deep neural network (Krizhevsky et al., 2012) brings visual learning into a new era. However, the performance heavily relies on the abundance of annotated data. Since traditional machine learning assumes a model is trained and verified in a fixed distribution, it cannot always be applied to real-world problems directly. Take image classification as an example, a number of factors, such as the change of light, noise, angle in which the image is pictured, and different types of sensors, can lead to a domain gap that harms the performance when predicting on test data. In many practical cases, a model trained in one or more source domains is desired that is also applicable to another domain. As a solution, domain adaptation (DA) aims to transfer the knowledge learned from a source distribution, which is typically fully labeled, into a different (but related) target distribution. This work focuses on the most challenging case, i.e., unsupervised domain adaptation (UDA), where no target label is available.

Ben-David et al. (2010) suggest that the target error can be minimized by bounding the error on source data, the discrepancy between distributions of the two domains, and a small optimal joint error. Optimal joint error is quantified by the lowest error rate that a hypothesis can possibly achieve on both domains, which also indicates the adaptability of a transfer learning problem. Many researchers focus on learning domain-invariant features such that the discrepancy can be minimized. For aligning distributions across domains, mainly two strategies have been substantially explored. The first one bridges the distributions by matching their statistics (Long et al., 2015; 2017; Pan et al., 2009). The second strategy utilizes adversarial learning (Goodfellow et al., 2014) to build a minimax game, where a domain discriminator is trained to distinguish the source from the target while the feature extractor is trained to confuse it simultaneously (Ganin & Lempitsky, 2015; Ganin et al., 2016; Tzeng et al., 2017). Despite the remarkable results achieved by distribution matching schemes, they still suffer from a major limitation: the joint distributions of feature spaces and categories are not well aligned across domains. As reported in Ganin et al. (2016), such methods fail to generalize in closely related source/target pairs, e.g., the adaptation from MNIST to SVHN. One

potential reason is when matching marginal distributions between two domains, samples from different classes can get mixed together. In this case, the joint error becomes non-negligible since no hypothesis can jointly classify source and target data with high accuracy.

This work aims to address the above problem by incorporating the joint error to formalize an optimizable upper bound such that the undesired overlap due to a wrong match can be properly penalized. UDA classification problems can be perfectly solved if we can match the conditional distributions of each class for source and target domain. In practice, however, most of the existing methods choose to deal with marginal distributions as we lack target labels (Ganin et al., 2016; Tzeng et al., 2017; Saito et al., 2017b; Zhang et al., 2019b; Kim et al., 2019). Motivated by this, we come up with a specially designed distance measurement, namely cross margin discrepancy, that leads our proposed upper bound to an objective that resembles CGAN [1] (a way to match conditional distributions) (Mirza & Osindero, 2014). We evaluate our proposal on several different classification tasks. In most experimental settings, our method improves the performance by a large margin. The contributions of this work can be summarized as follows:

- We propose a novel objective that relates to an upper bound of the joint error and show that our proposal can reduce the chance of misalignment through the marginal distribution matching.
- We construct a specific hypothesis space induced by source/pseudo-target labels to tighten up the proposed objective so that we can avoid optimizing a loose bound within an immense searching space.
- We adopt a novel measurement, namely cross margin discrepancy, that measures the dissimilarity between hypotheses. We show that using this novel measurement, we can alleviate the instability during adversarial learning.
- We present extensive empirical evidence showing that our proposal gives more reliable performance in image classification on several domain adaptation benchmarks compared with other upper bound related methods.

2 Related Work

The upper bound proposed by Ben-David et al. (2010) invoked numerous approaches focusing on reducing the gap between source and target domains by learning domain-invariant features, which can be achieved through statistical moment matching. Maximum Mean Discrepancy (MMD) (Long et al., 2015; 2017) is used to match the hidden representations of certain layers in a deep neural network. Transfer Component Analysis (TCA) (Pan et al., 2011) tries to learn a subspace across domains in a Reproducing Kernel Hilbert Space (RKHS) using MMD that dramatically minimizes the distance between domain distributions. Adaptive batch normalization (AdaBN) (Li et al., 2018) modulates the statistics from source to target on batch normalization layers across the network in a parameter-free way.

Another way to learn domain-invariant features is by leveraging generative adversarial network to produce target features that exactly match the source. Ganin & Lempitsky (2015) relax divergence measurement in the upper bound by a worst case which is equivalent to the maximum accuracy that a discriminator can possibly achieve when distinguishing source from target. Tzeng et al. (2017) follow this idea but separate the training procedure into classification stage and adversarial learning stage where an independent feature extractor is used for target. Saito et al. (2017b) explore a tighter bound by explicitly utilizing task-specific classifiers as discriminators such that features near the support of source samples will be favored by extractor. Zhang et al. (2019b) introduce margin disparity discrepancy, a novel measurement with rigorous generalization bounds, tailored to the distribution comparison with the asymmetric margin loss to bridge the gap between theory and algorithm. Methods that perform distribution alignment on pixel-level in raw input, which is known as image-to-image translation, are also proposed (Liu & Tuzel, 2016; Bousmalis et al., 2017; Sankaranarayanan et al., 2017; Shrivastava et al., 2016; Hoffman et al., 2018; Murez et al., 2017).

Distribution matching can not only bring the source and target domains closer, but also mix samples from different classes together. Therefore, Sener et al. (2016); Zhang et al. (2018) aim to use pseudo labels to

[1] In Eq.10, we show that our proposal includes a CGAN objective that aligns three pairs of hypothesis induced distributions

learn target discriminative representations which encourage a low-density separation between classes in the target domain (Lee, 2013). However, this usually requires auxiliary data-dependent hyper-parameters to set a threshold for reliable predictions. Long et al. (2018) present conditional adversarial domain adaptation, a principled framework that conditions adversarial adaptation models on the discriminative information conveyed in classifier predictions. However, it matches the marginal distributions of the joint distribution of inputs and pseudo predictions between domains which requires an balanced label assumption to achieve the alignment between conditional distributions. Wu et al. (2019) raise attention to the arbitrary increase in the joint error caused by distribution matching and propose a relaxed match by restricting the power of domain classifier to deal with the label shifting problem. However, it requires an overlap between the source and target domain in the input space and does not necessarily reduce the joint error. Saito et al. (2017a) claims their proposal can also reduce the joint error along with the discrepancy between domains by progressively building a pseudo labeled target set. However, it reforms the joint error as the sum of the error on the source and pseudo labeled target domain and a false label rate which can not be optimized. In this work, we present a theoretical approach that constructs an optimizable upper bound on the joint error for UDA.

In summary, the upper bound proposed by Ben-David et al. (2010) and its extensions (Ganin et al., 2016; Tzeng et al., 2017; Saito et al., 2017b; Zhang et al., 2019b) keep making progress in aligning the marginal distributions between the source and target domains. Nevertheless, the problem of ignoring the joint error remains unsolved. In the following sections, we will theoretically explain how this can harm the performance of the distribution matching in domain adaptation and why our proposal can tackle the problem.

3 Proposed Method

In this section, we present the details of our proposal. Firstly, in Sec.3.1 we give our base upper bound and show how it relates to the joint error. Then we provide more specific reasons on the necessity of the joint error theoretically. Secondly, in Sec.3.2 we explain how different choices of hypothesis spaces can affect the optimization of an objective. Finally, in Sec.3.3 we propose a novel measurement for the dissimilarity between hypotheses with a theoretical interpretation and demonstrate its utility in adversarial learning.

3.1 An Upper Bound Incorporating Joint Error

We consider the unsupervised domain adaptation as a binary classification task (our proposal holds for multi-class case) where the learning algorithm has access to a set of n labeled points $\{(x_s^i, y_s^i) \in (X \times Y)\}_{i=1}^n$ sampled i.i.d. from the source domain S and a set of m unlabeled points $\{(x_t^i) \in X\}_{i=1}^m$ sampled i.i.d. from the target domain T. Let $f_S : X \to \{0, 1\}$ and $f_T : X \to \{0, 1\}$ be the optimal labeling functions on the source and target domains, respectively. Let ϵ (usually 0-1 loss) denote a distance metric between two functions over a distribution that satisfies the symmetry and triangle inequality. As a commonly used notation, the source error of a hypothesis $h : X \to \{0, 1\}$ in space H is the disagreement w.r.t. the true labeling function f_S under domain S, i.e., $\epsilon_S(h) := \epsilon_S(h, f_S)$. Similarly, we use $\epsilon_T(h)$ to represent the error of the target domain. **With these notations, we propose the following upper bound for target error**[2]:

$$\begin{aligned}\boldsymbol{\epsilon_T(h) &\leq \epsilon_S(h) + \epsilon_T(f_S, f_T) + \epsilon_S(f_S, f_T) + \epsilon_T(h, f_S) - \epsilon_S(h, f_T)} \\ \boldsymbol{&= \epsilon_S(h) + C_{S,T}(f_S, f_T, h)}\end{aligned} \tag{1}$$

For simplicity, we use $C_{S,T}(f_S, f_T, h)$ to denote $\epsilon_T(f_S, f_T) + \epsilon_S(f_S, f_T) + \epsilon_T(h, f_S) - \epsilon_S(h, f_T)$ which indicates the discrepancy between domains. The above upper bound is minimized when $h = f_S$, and it is equivalent to $\epsilon_T(f_S, f_T)$ owing to the triangle inequality[2]. Furthermore, we demonstrate in such case, **our proposal is equivalent to an upper bound of the optimal joint error**[2] λ.

The reason we focus on the joint error is that Ben-David et al. (2010) state the target error can be upper bounded by the sum of the source risk, the marginal discrepancy between the source and target distributions and the joint error:

$$\epsilon_T(h) \leq \epsilon_S(h) + \sup_{f_1, f_2 \in H} |\epsilon_S(f_1, f_2) - \epsilon_T(f_1, f_2)| + \lambda$$

[2]See proof in A.6

but plenty of works (Ganin et al., 2016; Tzeng et al., 2017; Saito et al., 2017b; Zhang et al., 2019b; Kim et al., 2019) choose to ignore λ and mainly focus on minimizing the marginal discrepancy within a transformed input space $S_g = \{(g(x_s), y_s)|(x_s, y_s) \sim S\}, T_g = \{g(x_t)|x_t \sim T\}$ introduced by a feature extractor g:

$$\min_{h,g:h\circ g\in H}[\epsilon_{S_g}(h) + \max_{f_1,f_2:f_1\circ g,f_2\circ g\in H} |\epsilon_{S_g}(f_1, f_2) - \epsilon_{T_g}(f_1, f_2)|] + \lambda_g$$

where the joint error $\lambda_g = \min_{h^*:h^*\circ g\in H} \epsilon_{S_g}(h^*) + \epsilon_{T_g}(h^*)$. In the original theory (Ben-David et al., 2010), the joint error is indeed an independent term. **However, when we introduce the feature extractor g to minimize the marginal discrepancy, we also break the independence. The joint error varies along with the change of g, and it can become non-negligible if samples from different classes in the source and target domain get mixed together especially when a huge domain gap exists** (Zhao et al., 2019). In that case, no matter how we minimize the marginal discrepancy, the target error is unbounded as not a single h can jointly classify both domains.

In Fig. 1b, we illustrate a case where common methods fail to penalize the undesirable situation. During the distribution matching it can happen that distributions of different classes get aligned together. While this does reduce the marginal discrepancy, it introduces a huge joint error. This can be seen in the right part of Fig. 1b, while the marginal discrepancy (areas 1, 3, 4 and 6) is relatively small, there is a large joint error (areas 2 and 5). In this case, reducing marginal discrepancy (areas 1, 3, 4 and 6) leads to an increasing joint error (areas 2 and 5). For the case shown in Fig. 1b, we assume f_S takes a specific form. As a result, $\epsilon_T(f_S, f_T)$ exactly measures the overlapping areas 2 and 5, which is equivalent to the optimal joint error. As the two areas represent the overlaps of different classes, there is no hypothesis that can correctly classify the samples in those areas, which leads to a non-negligible joint error. Our proposal is closely related to the optimal joint error and can adequately reduce the size of overlapping during the distribution matching. Additionally, we provide a Rademacher complexity bound in A.3 according to Mansour et al. (2009).

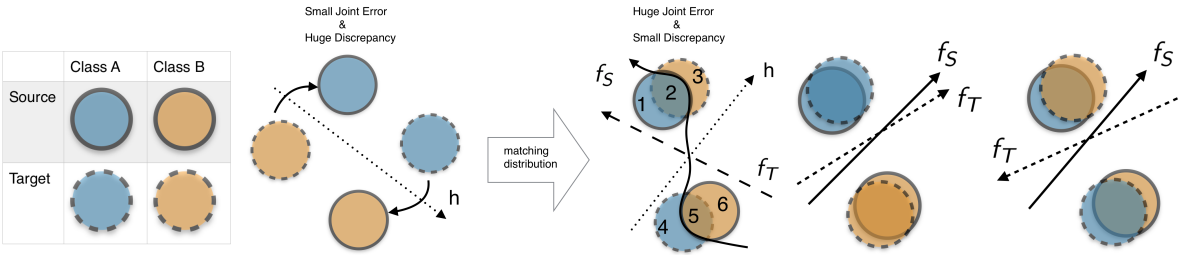

(a) legend (b) joint error (c) location of f_T

Figure 1: The left side of a classifier (arrow) is class A and the right side is class B; (a) Legend; (b) Joint error (areas 2 and 5) is penalized such that the feature extractor must try to avoid such an overlap; (c) even with the marginal distribution aligned f_S and f_T might be largely different.

3.2 Hypothesis Space Constraint

Since the optimal labeling functions f_S, f_T are not available during the training, **we shall further relax the upper bound Eq.1 by taking supremum** w.r.t f_S, f_T within a hypothesis space H[3]:

$$\boldsymbol{\epsilon_T(h) \leq \epsilon_S(h) + C_{S,T}(f_S, f_T, h) \leq \epsilon_S(h) + \sup_{f_1,f_2\in H} C_{S,T}(f_1, f_2, h)}$$

Then minimizing the upper bound of the target error $\epsilon_T(h)$ becomes optimizing a minmax game. However, as the max-player with **two classifiers $f_1, f_2 \in H$** is much stronger due to a larger searching space, we introduce **a feature extractor $g \in H_g$** and transformed feature space $\boldsymbol{S_g = \{(g(x_s), y_s)|(x_s, y_s) \sim S\}, T_g = \{g(x_t)|x_t \sim T\}}$ for the min-player to compensate for it (Now $f_1, f_2 \in H_f$ and $f_1 \circ g, f_2 \circ g \in H$).

[3]Our proposal holds even if $f_S, f_T \notin H$, which is proved in A.4

Applying g to both domains, **the overall objective can be written as**:

$$\boldsymbol{\min_{g \in H_g, h \in H_f} [\epsilon_{S_g}(h) + \max_{f_1, f_2 \in H_f} C_{S_g, T_g}(f_1, f_2, h)]}$$

However, if we leave H_f unconstrained, the maximum term can be arbitrarily large. In order to obtain a tight bound, we need to restrict the size of hypothesis space as well as maintain the upper bound. **We assume that it is possible to build two subspaces $\boldsymbol{H_1, H_2 \subseteq H_f}$ such that the following holds**:

$$\boldsymbol{C_{S_g, T_g}(f_S, f_T, h) \leq \max_{f_1 \in H_1, f_2 \in H_2} C_{S_g, T_g}(f_1, f_2, h) \leq \max_{f_1, f_2 \in H_f} C_{S_g, T_g}(f_1, f_2, h)} \tag{2}$$

The right side of the above inequality always holds because of the subspace relation. A sufficient condition for the left side inequality is $f_S \in H_1, f_T \in H_2$. The condition for H_1 can be easily achieved since we have source labels to construct a space consisting of all classifiers for the source domain, namely H_{sc} which must contain f_S. However, the condition for H_2 is a little problematic since we have no access to the true labels of the target domain, thus it is hard to locate f_T. Therefore, we construct a constrained hypothesis space for H_2 that most likely contains f_T. **Generally, it is hard to demonstrate the validity of the left side inequality of Eq.2 theoretically. Instead, we show experimental results of the real world problem to support our assumption**[4].

As illustrated in Fig. 1c, if the conditional distributions are well-aligned (e.g., left side of Fig. 1c) after the matching between the source and target domain, it is fair to assume that $f_T \in H_{sc}$. However, a good alignment might not always hold true, especially when samples from different classes are mixed together (e.g., right side of Fig. 1c). Considering this, **we propose a training objective in the following sections based on the constraints for $\boldsymbol{H_2}$** which aim to alleviate the worst case caused by the unknown location of f_T.

3.2.1 Target-driven Hypothesis Space (THS)

We first build a space where the hypothesis can classify all the samples from the source domain, namely H_{sc}. Then, we build a space consisting of all classifiers for the approximated target domain $\{(x_t^i, h(x_t^i)) \in X \times Y\}_{i=1}^m$ based on pseudo labels which can be obtained by predictions of h during the training procedure, namely $H_{\tilde{t}c}$. **We further define $\boldsymbol{H_2}$ as an intersection between two hypothesis spaces, i.e., $\boldsymbol{H_{sc}^{\gamma} \cap H_{\tilde{t}c}^{1-\eta}}$** where the hypothesis can classify samples from the source domain with an accuracy of $\gamma \in [0, 1]$ and classify samples from the approximated target domain with an accuracy of $1 - \eta \in [0, 1]$ (**usually, we set $\boldsymbol{\gamma = \eta}$ for simplicity; however, in some experiments we tune the two parameters to show the influence when restricting the belief towards the source predictions and leveraging the pseudo predictions**). In practice, it is difficult to actually build such a space and sample from it due to a huge computational cost. Instead, we use a weighted average loss to constrain the behavior of f_2 as an approximation to the sample from $H_{sc}^{\gamma} \cap H_{\tilde{t}c}^{1-\eta}$, which allows us to use η to balance the confidence towards the source and pseudo target domain. This leads to the following training objective:

$$\begin{cases} \boldsymbol{\min_{g \in H_g, h \in H_f} [\epsilon_{S_g}(h) + \max_{f_1 \in H_1, f_2 \in H_2} C_{S_g, T_g}(f_1, f_2, h)]} \\ \text{s.t.} \quad \boldsymbol{H_1, H_2 = \{f_1, f_2 | \arg\min_{f_1, f_2 \in H_f, g \in H_g} [\epsilon_{S_g}(f_1) + \gamma \epsilon_{S_g}(f_2) + (1 - \eta) \tilde{\epsilon}_{T_g}(f_2)]\}} \end{cases} \tag{3}$$

3.2.2 Intuition to the Difference between Hypothesis Spaces

The reason we put the above constraints on hypothesis space H_2 can be intuitively explained by Fig. 2. If we confine the hypothesis space H_2 to H_{sc} (a set of classifiers for all source samples), the classifier $f_2 \in H_2$ is forced to correctly classify all source samples. As a result, it increases the chance that all target samples are outside the decision boundary of f_2 especially when the domain shift is huge. In this case, the feature extractor could move the samples into either side of the decision boundary of f_2 to reduce the objective

[4]We show that our proposal remains a valid upper bound even if the domain gap is so large that we are not likely to construct a hypothesis space that contains f_T in A.5

$\epsilon_T(f_1, f_2)$ (shadow area in Fig. 2a) which may cause a wrong alignment. By constructing H_2 as a intersection of two hypothesis space H^{γ}_{sc} (a set of classifiers for a part of source samples), $H^{1-\eta}_{\tilde{t}c}$ (a set of classifiers for a part of pseudo labeled target samples) in Fig. 2b, we alleviate restrictions on f_2 which makes it more likely that the decision boundary passes at least through some target samples, where the feature extractor can properly reduce the objective (shadow area) by moving those samples toward the inside of the decision boundary of f_2. Besides, given these hypothesis space constraints, **we demonstrate that under some conditions, our proposal reduces to some other UDA methods**[5].

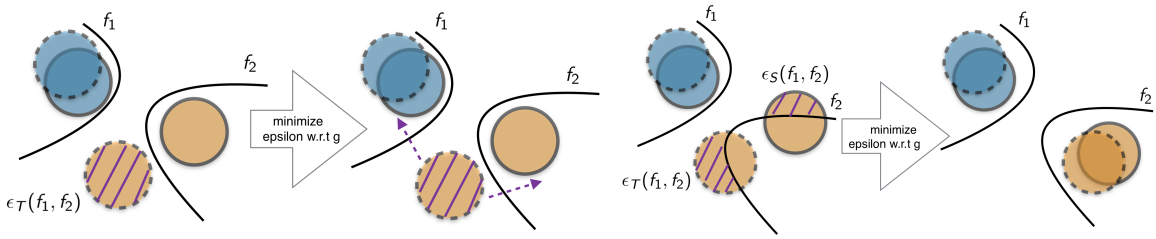

(a) $H_2 = H_{sc}$ (b) $H_2 = H^{\gamma}_{sc} \cap H^{1-\eta}_{\tilde{t}c}$

Figure 2: An improper hypothesis space constrain can cause wrong alignment. (a) If f_2 is forced to only classify all source samples, it may completely misclassify all target samples when the domain shift is huge; (b) If f_2 can classify a part of source samples and pseudo labeled target samples, the feature extractor can align the distributions in a desired way by minimizing the upper bound (shadow area).

3.3 Cross Margin Discrepancy (CMD)

In this section, inspired by margin theory, **we propose a novel discrepancy measurement named cross margin discrepancy for ϵ** instead of those commonly used ones (e.g., logistic, hinge, L_1) to stabilize the training of adversarial learning. Following the above notations, we define a measurement of the discrepancy between two hypotheses f_1, f_2 (e.g., a multi-layer perceptron whose output layer is a softmax function) over a distribution D:

$$\boldsymbol{\epsilon_D(f_1, f_2) = \mathbb{E}_{x \in D}[\mathrm{cmd}(f_1, f_2; x)]} \tag{4}$$

Then we consider a score function $s(y|x)$ for multi-class classification where the output indicates the confidence of the prediction on class y. Thus an induced labeling function named l_s from $X \to Y$ is given by:

$$l_s : x \to \arg\max_{y \in Y} s(y|x)$$

When the two hypotheses (f_1, f_2) disagree on x, i.e., $y_1 = l_{f_1}(x) \neq l_{f_2}(x) = y_2$, the loss is defined as:

$$\mathbf{cmd}(f_1, f_2, x) = \log f_1(y_1|x) + \log(1 - f_1(y_2|x)) + \log f_2(y_2|x) + \log(1 - f_2(y_1|x)) \tag{5}$$

where we refer to $\log f(y|x)$ as the **positive** part and $\log(1 - f(y|x))$ as the **negative** part.

When the two hypotheses (f_1, f_2) agree on x, i.e., $y = l_{f_1}(x) = l_{f_2}(x)$, the loss is defined as:

$$\mathbf{cmd}(f_1, f_2; x) = \log \max(f_1(y|x), f_2(y|x)) + \log \max(1 - f_1(y|x), 1 - f_2(y|x)) \tag{6}$$

We demonstrate that CMD can be view as a sum of two well-established margin losses[6], which play a significant role in achieving strong generalization performance (Koltchinskii & Panchenko, 2002), **as well as a training objective of CGAN**[7], which is an efficient way to align conditional distributions

[5]See proof in A.2
[6]See proof in A.8
[7]See proof in A.9

(Mirza & Osindero, 2014). Another reason why we propose such a discrepancy measurement is that **it helps alleviate the instability in adversarial learning**. As illustrated in Fig. 3b, during the optimization of a minimax game, when two hypotheses try to maximize the discrepancy (striped area), if one moves too fast around the decision boundary such that the discrepancy is actually maximized w.r.t some samples, then these samples can be moved into either side to decrease the discrepancy by tuning the feature extractor. From Fig. 3a, it can be seen that CMD is flat for the points around the original, i.e., the gradient w.r.t those points near the decision boundary will be relatively small, which can help to prevent the above failure as each update of a hypothesis will be subtle during the training.

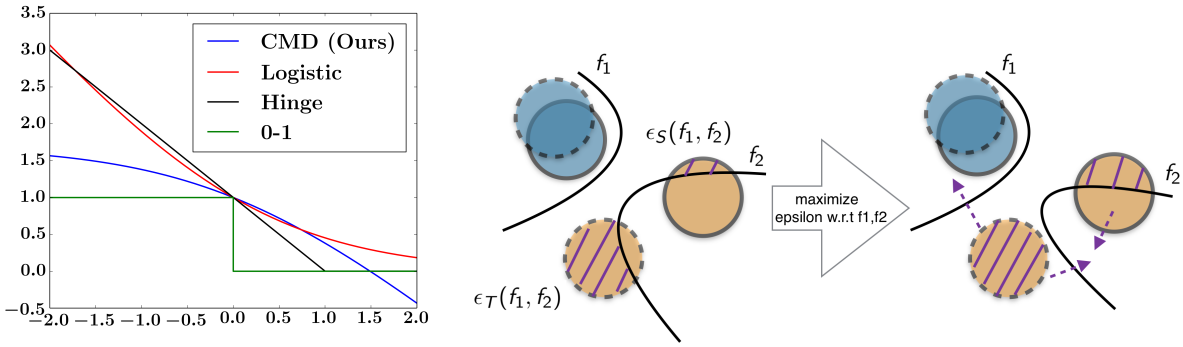

(a) loss curve

(b) instability

Figure 3: (a) Loss of binary classification where ours shows small gradient around the original; (b) Steep gradients near the original may lead to an extreme move of the decision boundary.

3.4 Training Procedure

This section briefly explains the training procedure of the proposed method, which follows a similar pipeline proposed by Saito et al. (2017b). Here we take THS objective (Eq.3) as an example and each term is clearly defined below, where g represents a feature extractor and h, f_1, f_2 are classifiers with a softmax output. **A simple implementation to achieve hypothesis space constraints is to use the cross-entropy loss**[8]:

$$\begin{cases} \boldsymbol{\epsilon_{S_g}(f_1) = -\mathbb{E}_{x,y\sim S_g} \log(f_1(y|x))} \\ \boldsymbol{\gamma\epsilon_{S_g}(f_2) + (1-\eta)\tilde{\epsilon}_{T_g}(f_2) = -\gamma\mathbb{E}_{x,y\sim S_g} \log(f_2(y|x)) - (1-\eta)\mathbb{E}_{x\sim T_g} \log(f_2(l_h(x)|x))} \end{cases} \tag{7}$$

Then we define the discrepancy term with the proposed cross margin discrepancy(Eq.1, Eq.4, Eq.5, Eq.6):

$$\boldsymbol{C_{S_g,T_g}(f_1, f_2, h)) = \mathbb{E}_{x\sim T_g}[\mathrm{cmd}(f_1, f_2; x) + \mathrm{cmd}(h, f_1; x)] + \mathbb{E}_{x\sim S_g}[\mathrm{cmd}(f_1, f_2; x) - \mathrm{cmd}(h, f_2; x)]} \tag{8}$$

Following the procedure described in Fig.4 and Alg.1, for a mini-batch of input, during one training cycle, we firstly train g, f_1, f_2 to satisfy the hypothesis space constraint; secondly, we introduce a trade-off hyper-parameter $\lambda = 0.01$ to balance the source error and discrepancy then train f_1, f_2 to maximize the discrepancy term within the hypothesis space constraint; finally, we train g, h to minimize the entire upper bound. We use $\hat{C}, \check{C}$ to emphasize the difference of the discrepancy term optimized in different steps such that the objective is consistent with GAN (**the positive part of CMD is fixed in Step C**). Step C is executed 4 times inside a training cycle according to Saito et al. (2017b). See A.9 for more details of the objective.

4 Evaluation

In this section, we perform an extensive evaluation on image classification for several different datasets (Digit (Netzer et al., 2011; LeCun et al., 1998; Hull, 1994), VisDA (Peng et al., 2017), Office-Home (Venkateswara

[8]Here, for simplicity, we estimate $\tilde{\epsilon}_{T_g}(f_2)$ with a pseudo label based cross-entropy loss; however, in complex datasets, we usually introduce some regularization terms to prevent f_2 from over-fitting noisy pseudo labels (A.1.3, Eq.9)

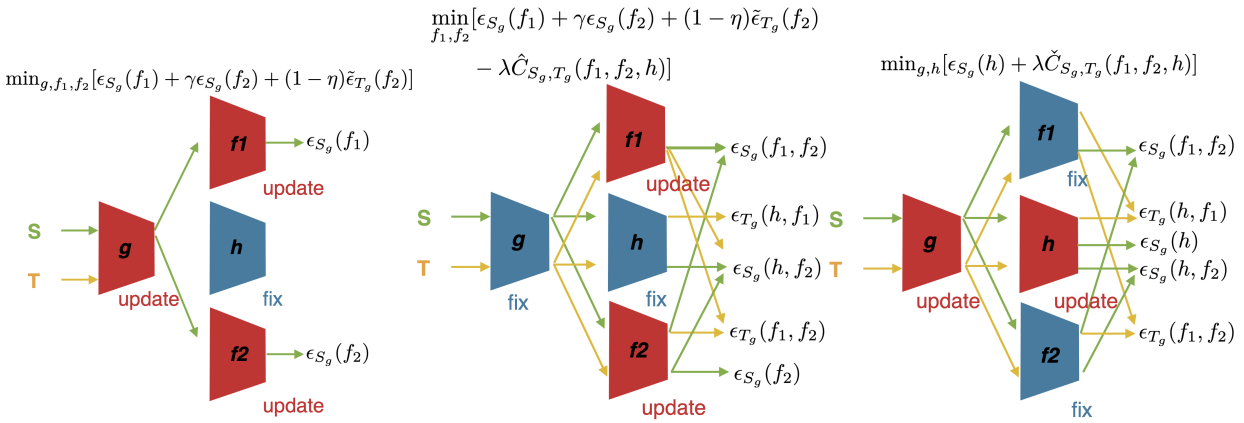

(a) Step A (b) Step B (c) Step C

Figure 4: Training procedure of the proposed method: (i) Train g, f_1, f_2 to satisfy the hypothesis space constraint; (ii) Train f_1, f_2 to maximize the discrepancy within the hypothesis space constraint; (iii) Train g, h to minimize the entire upper bound.

Table 1: Accuracy of models adapted on digits datasets (* denotes the whole training set)

METHOD	SVHN to MNIST	MNIST to SVHN	MNIST to USPS	MNIST* to USPS*	USPS to MNIST
Source Only	67.1	21.3	76.7	79.7	63.4
MDD†(Long et al., 2015)	71.1	-	-	81.1	-
DANN†Ganin et al. (2016)	71.1	25.1	77.3	85.1	73.2
DRCN(Ghifary et al., 2016)	82.0±0.1	40.1±0.1	91.8±0.1	-	73.7±0.1
ADDA(Tzeng et al., 2017)	76.0±1.8	-	89.4±0.2	-	90.1±0.8
MCD(Saito et al., 2017b)	96.2±0.4	11.2±1.1	94.2±0.7	96.5±0.3	94.1±0.3
GPDA(Kim et al., 2019)	98.2±0.1	-	96.5±0.2	98.1±0.1	96.4±0.1
ours ($THS + L_1, \gamma = \eta = 1$)	96.8±0.2	30.4±1.5[9]	94.5±0.3	96.8±0.3	95.2±0.2
ours ($THS + CMD, \gamma = \eta = 1$)	97.5±0.2	31.5±1.8[9]	95.3±0.3	97.2±0.2	95.6±0.2
ours ($THS + CMD, \gamma = \eta = 0.9$)	98.6±0.1	50.3±1.3	96.8±0.2	97.9±0.1	96.9±0.1

et al., 2017), Office-31 (Saenko et al., 2010)) to verify the effectiveness of our proposal. We choose MCD (Saito et al., 2017b) as a baseline for the major comparisons with ours because the two methods share the same concept, which is to tighten the upper bound established by Ben-David et al. (2010). Besides, the two methods utilize the same network architecture and training procedure, which makes the results fairly comparable. We conduct an ablation study (A.11) to show the contribution of each part of our proposal. We manually create an imbalance label situation and show the robustness of our proposal (A.10). Details of the experimental settings, the hyper-parameter selection and the training objective are provided in A.1, A.7, A.9.

4.1 Experiment on Digit Dataset

In this experiment, our proposal is assessed in four types of adaptation scenarios by adopting commonly used digits datasets, i.e., MNIST (LeCun et al., 1998), Street View House Numbers (SVHN) (Netzer et al., 2011), and USPS (Hull, 1994) such that the result can be easily compared with other popular methods. All experiments are performed in an unsupervised fashion without any kinds of data augmentation. We report the accuracy of different methods in Tab. 1. Our proposal manages to improve the performance in almost all settings except for a single result compared with GPDA (Kim et al., 2019). However, their solution requires

[9]We use $\gamma = 0.1$ for MNIST $\rightarrow$ SVHN

Algorithm 1 MJE

Input: source data S and unlabeled target data T
Parameter: constrained classifiers f_1, f_2; shared feature extractor g; upper bound classifier h; hyper-parameters λ, η; learning rate α
Output: updated parameters g, h
for *iteration* $= 1, 2, \ldots$ **do** Randomly sample 2 mini-batch s, t of the same size from the source (S) and unlabeled target (T) domains respectively

Step 1: optimize g, f_1, f_2 to satisfy the hypothesis constraint (Eq.7)
Compute the classification loss required by the hypothesis space constraint:

$$L_f = -\mathbb{E}_{(x,y)\in s}[\log(f_1(y|g(x))) + \eta \log(f_2(y|g(x)))] \\ - \mathbb{E}_{x\in t}[(1-\eta)\log(f_2(l_{h(x)}|g(x)))]$$

Update g, f_1, f_2:
$(g, f_1, f_2) \leftarrow (g, f_1, f_2) + \alpha\Delta(g, f_1, f_2)$ where $\Delta(g, f_1, f_2) = -\frac{\partial L_f}{\partial(g, f_1, f_2)}$

Step 2: maximize the conditional discrepancy w.r.t. f_1, f_2 within the hypothesis space constraint
Compute the classification loss L_f required by the hypothesis space constraint as above
Compute the conditional discrepancy based on CMD (Eq.5, Eq.6):

$$C_{s_g,t_g}(f_1, f_2, h) = \mathbb{E}_{x\in t}[\text{cmd}(f_1, f_2; g(x)) + \text{cmd}(f_1, h; g(x))] \\ + \mathbb{E}_{x\in s}[\text{cmd}(f_1, f_2; g(x)) - \text{cmd}(f_2, h; g(x))]$$

Update f_1, f_2:
$(f_1, f_2) \leftarrow (f_1, f_2) + \alpha\Delta(f_1, f_2)$ where $\Delta(f_1, f_2) = -\frac{\partial(L_f - \lambda C_{s_g,t_g}(f_1,f_2,h))}{\partial(f_1,f_2)}$

Step 3: minimize the entire target error upper bound w.r.t. g, h for fixed f_1, f_2 (Eq.3)
Compute the classification loss for the entire task:

$$L_h = -\mathbb{E}_{(x,y)\in s}\log(h(y|g(x)))$$

Compute the conditional discrepancy $C_{s_g,t_g}(f_1, f_2, h)$ as above
Update g, h:
$(g, h) \leftarrow (g, h) + \alpha\Delta(g, h)$ where $\Delta(g, h) = -\frac{\partial(L_h + \lambda C_{s_g,t_g,}(f_1,f_2,h))}{\partial(g,h)}$

end for

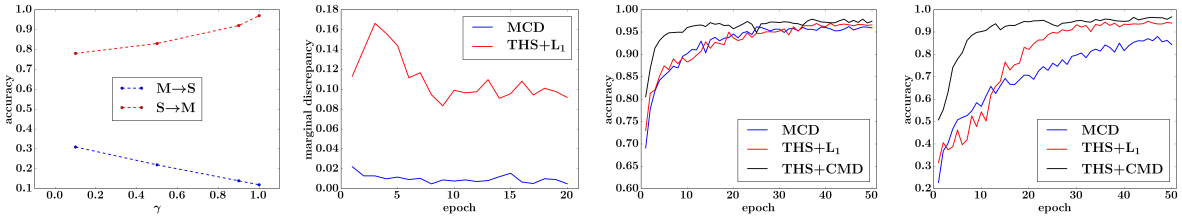

(a) domain gap affects γ (fixed $\eta = 1$) (b) M→S (c) S→M (d) M→U

Figure 5: (a) Sensitivity w.r.t. γ; (b) Comparisons for marginal discrepancy; (c)-(d) Comparisons for convergence rate; All plots are drawn based on the average of 3 runs.

sampling that increases data size and is equivalent to adding Gaussian noise to the last layer of a classifier, which is considered as a type of augmentation. The first setting of our proposal $THS + L_1$ where $\gamma = \eta = 1$ serves as a direct comparison to MCD since the two methods share the same architecture except the upper

Table 2: Accuracy of ResNet-101 model fine-tuned on VisDA dataset within 10 epochs

METHOD	plane	bcycl	bus	car	horse	knife	mcycl	person	plant	sktbrd	train	truck	avg
Source Only	55.1	53.3	61.9	59.1	80.6	17.9	79.7	31.2	81.0	26.5	73.5	8.5	52.4
MDD(Long et al., 2015)	87.1	63.0	76.5	42.0	90.3	42.9	85.9	53.1	49.7	36.3	85.8	20.7	61.1
DANN(Ganin et al., 2016)	81.9	77.7	82.8	44.3	81.2	29.5	65.1	28.6	51.9	54.6	82.8	7.8	57.4
MCD(Saito et al., 2017b)	87.0	60.9	83.7	64.0	88.9	79.6	84.7	76.9	88.6	40.3	83.0	25.8	71.9
GPDA(Kim et al., 2019)	83.0	74.3	80.4	66.0	87.6	75.3	83.8	73.1	90.1	57.3	80.2	37.9	73.3
MCCJin et al. (2020)	88.1	80.3	80.5	71.5	90.1	93.2	85.0	71.6	89.4	73.8	85.0	36.9	78.8
ours ($THS + L_1, \gamma = \eta = 1$)	86.3	82.7	83.7	68.7	87.9	72.7	85.4	61.5	87.3	55.5	75.2	34.1	73.4
ours ($THS + CMD, \gamma = \eta = 1$)	88.4	83.3	74.8	78.0	88.1	43.2	88.2	68.9	87.6	65.5	92.6	58.5	76.4
ours ($THS + CMD, \gamma = \eta = 0.9$)	93.8	79.5	79.3	55.9	93.9	93.8	86.5	80.3	91.6	87.7	85.4	51.6	81.6

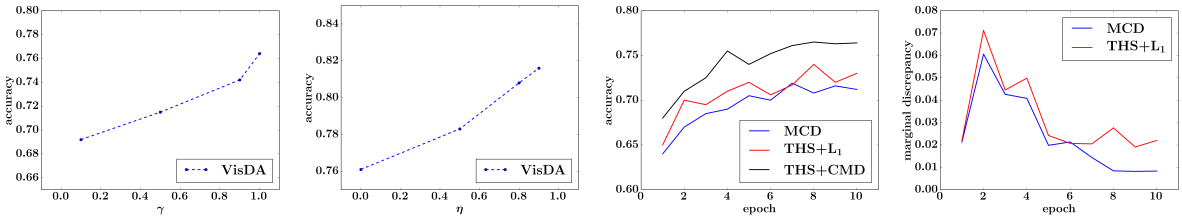

(a) fixed $\eta = 1$ (b) various values for $\gamma = \eta$ (c) faster convergence (d) higher discrepancy

Figure 6: (a)-(b) Sensitivity w.r.t. γ,η; (c) Comparisons for convergence rate; (d) Comparisons for marginal discrepancy; All plots are drawn based on the average of 3 runs.

bound, which demonstrates the importance of the joint error. The second and third setting of our proposal shows the influence of the cross margin discrepancy and hypothesis space constraint.

Fig. 5a shows the result when we fix $\eta = 1$ and it can be seen that the hyper-parameter γ is quite sensitive to the domain gap. In short, setting $\gamma = 1$ yields the best performance in most situations, since f_S, f_T can be quite close after aligning distributions, especially in these easily adapted scenarios. However, in MNIST $\rightarrow$ SVHN, setting $\gamma = 0.1$ gives the optimum which means that f_S, f_T are so far away due to a huge domain gap that no extractor is capable of introducing an identical conditional distribution in feature space. Besides, we test the performance on different values for $\gamma = \eta \neq 1$ setting then find out that the accuracy remains high and varies subtly, therefore we omit a figure for it. Furthermore, Fig. 5b empirically proves simply minimizing the discrepancy between marginal distributions does not necessarily lead to a reliable adaptation. In addition, Fig. 5c and Fig. 5d show the effectiveness of the cross margin discrepancy which accelerates the convergence and provides a slightly better result.

4.2 Experiment on VisDA Dataset

The VisDA dataset (Peng et al., 2017) is designed for 12-class adaptation task from synthetic object to real object images. Source domain contains 152,397 synthetic images generated by rendering 3D CAD models and target domain is collected from MSCOCO (Lin et al., 2014) consisting of 55,388 real images. We report the accuracy of different methods in Tab. 2, and find that our proposal works well in all settings. The image structure of this dataset is more complex than that of digits, yet our method provides reliable performance even under such a challenging condition. Another key observation is that some competing methods (e.g., DANN, MCD), which can be categorized as distribution matching based on adversarial learning, perform worse than MDD (which simply matches statistics) in classes such as plane and horse, while our methods perform better across all classes. This clearly demonstrates the importance of the joint error. Fig. 6a shows the result when we fix $\eta = 1$ and the performance drops when relaxing the constraint which actually confuses us. Because we expect an improvement here since it is hard to believe that f_S, f_T eventually lie in a similar space judging from the relatively low prediction accuracy. Fig. 6b shows the adaptation performance of different values for $\gamma = \eta \neq 1$ setting and the prediction accuracy drops when η goes below 0.9. One possible cause is that f_2 and h might almost agree on the target domain, such that the prediction of h cannot provide

Table 3: The accuracy of ResNet-50 model fine-tuned on the Office-Home dataset. We repeated each experiment 5 times and report the average of the accuracy.

METHOD	Ar→Cl	Ar→Pr	Ar→Rw	Cl→Ar	Cl→Pr	Cl→Rw	Pr→Ar	Pr→Cl	Pr→Rw	Rw→Ar	Rw→Cl	Rw→Pr	Avg
Source Only	34.9	50.0	58.0	37.4	41.9	46.2	38.5	31.2	60.4	53.9	41.2	59.9	46.1
DANN(Ganin et al., 2016)	45.6	59.3	70.1	47.0	58.5	60.9	46.1	43.7	68.5	63.2	51.8	76.8	57.6
MCD(Saito et al., 2017b)	51.9	70.7	74.8	59.0	68.4	68.8	58.2	51.6	75.1	69.5	55.8	79.3	65.3
CDAN(Long et al., 2018)	50.7	70.6	76.0	57.6	70.0	70.0	57.4	50.9	77.3	70.9	56.7	81.6	65.8
SymNets(Zhang et al., 2019a)	47.7	72.9	78.5	64.2	71.3	74.2	64.2	48.8	79.5	74.5	52.6	82.7	67.6
SPL(Wang & Breckon, 2020)	54.5	77.8	81.9	65.1	78.0	81.1	66.0	53.1	82.8	69.9	55.3	86.0	71.0
AADA(Yang et al., 2020)	54.0	71.3	77.5	60.8	70.8	71.2	59.1	51.8	76.9	71.0	57.4	81.8	67.0
SRDC(Tang et al., 2020)	52.3	76.3	81.0	69.5	76.2	78.0	68.7	53.8	81.7	76.3	57.1	85.0	71.3
SCAL(Wang et al., 2022)	55.3	72.7	78.7	63.1	71.7	73.5	61.4	51.6	79.9	72.5	57.8	81.0	68.3
ours ($THS + CMD, \gamma = \eta = 0.9$)	60.3	77.8	81.0	66.0	74.4	74.5	66.7	59.3	81.8	74.2	62.7	84.9	72.0

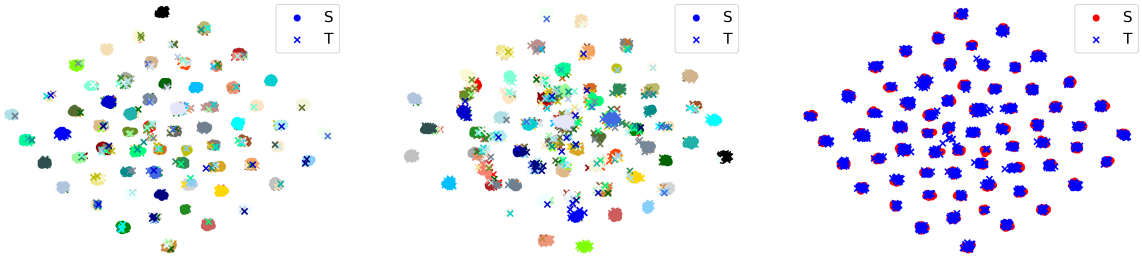

(a) conditional discrepancy (ours) (b) conditional discrepancy (MCD) (c) marginal discrepancy (ours)

Figure 7: Feature visualization with t-SNE in scenario Real to Art; (a)-(b) shows the conditional discrepancy by using different colors for each class; (c) shows the marginal discrepancy by using the same color for the all classes.

more accurate information of the target domain without introducing noisy pseudo labels. Fig. 6c and Fig. 6d again demonstrate the effectiveness of the cross margin discrepancy and the importance of the joint error.

4.3 Experiment on Office-Home Dataset

Office-Home (Venkateswara et al., 2017) is a complex dataset containing 15,500 images from four significantly different domains: Art (Ar), Clipart (Cl), Product (Pr) and Real-World (Rw). We report the accuracy of different methods in Tab. 3. From the table, it can be seen that the adaptation accuracy of the source-only method is rather low, which means a huge domain gap is quite likely to exist. In such case, we believe simply minimizing the discrepancy between the source and target domain may not work as the joint error can increase when aligning the distributions. As reported, our proposal gives better performance in general when the adaptation is hard (1st, 8th and 11th columns). This result suggests that our proposal which incorporates the joint error into the target error upper bound can boost the performance especially when there is a large domain gap. SPL (Wang & Breckon, 2020) and SRDC (Tang et al., 2020) share a similar strategy which can be described as cluster based iterative pseudo labeling. Despite the outstanding performance, their methods lack a theoretical guarantee on the generalization error bound. Besides, they assume samples in the target domain are well clustered within the feature space and can be labeled by the euclidean distance from clusters obtained with K-means. As for the first assumption, it is not always true since the high dimensional features can lie in a low dimensional manifold (e.g., Swiss Roll dataset) where no cluster exists. As for the second assumption, the labeling scheme can be vulnerable because K-means is sensitive to the initialization and the euclidean distance can suffer from the curse of dimensionality where there is little difference in the distances between different pairs of samples. After all, this work aims to demonstrate the necessity of joint error especially when the domain gap is huge; thus further discussion on the pseudo labeling strategies is beyond the scope of this work.

In addition, we plot the learned features with t-SNE (van der Maaten & Hinton, 2008) in Fig. 7 which shows the scenario of Real to Art . In Fig. 7a, we illustrate the source (dot) and target (cross) features with

Table 4: The accuracy of ResNet-50 model fine-tuned on the Office-31 dataset. We repeated each experiment 5 times and report the average and the standard deviation of the accuracy.

METHOD	A→W	D→W	W→D	A→D	D→A	W→A	AVG
SOURCE ONLY	68.4±0.2	96.7±0.1	99.3±0.1	68.9±0.2	62.5±0.3	60.7±0.3	76.1
DANN(GANIN ET AL., 2016)	82.0±0.4	96.9±0.2	99.1±0.1	79.7±0.4	68.2±0.4	67.4±0.5	82.2
ADDA(TZENG ET AL., 2017)	86.2±0.5	96.2±0.3	98.4±0.3	77.8±0.3	69.5±0.4	68.9±0.5	82.9
MCD(SAITO ET AL., 2017B)	88.6±0.2	98.5±0.1	100.0±.0	92.2±0.2	69.5±0.1	69.7±0.3	86.5
CDAN(LONG ET AL., 2018)	94.1±0.1	98.6±0.1	100.0±.0	92.9±0.2	71.0±0.3	69.3±0.3	87.7
SYMNETS(ZHANG ET AL., 2019A)	90.8±0.1	98.8±0.3	100.0±0.0	93.9±0.5	74.6±0.6	72.5±0.5	88.4
SPL(WANG & BRECKON, 2020)	92.7±0.0	98.1±0.0	99.8±0.0	93.7±0.0	76.4±0.0	76.9±0.0	89.6
MCC(JIN ET AL., 2020)	95.5±0.2	98.6±0.1	100.0±0.0	94.4±0.3	72.9±0.2	74.9±0.3	89.4
SRDC(TANG ET AL., 2020)	94.6±1.0	99.2±0.5	100.0±0.0	92.6±0.6	78.1±1.3	76.3±0.2	90.1
SCAL(WANG ET AL., 2022)	93.5±0.2	98.5±0.1	100.0±0.0	93.4±0.3	72.4±0.1	74.0±0.3	88.6
OURS ($THS + CMD, \gamma = \eta = 0.9$)	91.9±0.5	99.0±0.2	100.0±.0	93.7±0.5	76.1±0.2	77.8±0.2	89.8

different colors that represent their classes. In our method, most of the target features are clustered to their corresponding sources and do not show a large variance from the class center compared to MCD (Fig. 7b). We also visualize features of the source (red dot) and target (blue cross) domain in Fig. 7c to show the entire domain discrepancy. It can be seen that the target features are also well-aligned with those of the source domain.

4.4 Experiment on Office-31 Dataset

Office-31 (Saenko et al., 2010) is a popular dataset to verify the effectiveness of a domain adaptation algorithm, which contains three diverse domains: Amazon (A), Webcam (W) and DSLR (D) with 4,652 images in 31 unbalanced classes. The results on Office-31 are reported in Tab. 4. As for the tasks D→A and W→A, judging from the relatively low adaptation accuracy across all methods, it is quite likely that there is a huge domain gap between the source and target domain. Our method works well in such cases which demonstrates that the proposal manages to penalize the undesired matching between the source and target domain. However, the advantage is not remarkable especially for the task A→W, where our proposal shows relatively high variance and poor performance. One possible reason is that our method depends on building reliable classifiers for the source domain to satisfy the constraint for the hypothesis space. However, the Amazon domain contains a lot of noise and the entire dataset lacks diversity (e.g., some domains only have several hundred samples with many duplicates) which makes it difficult for a traditional error bound based method that usually requires a sufficient sample size to learn a reliable classifier.

5 Conclusion

In this work, we propose a novel upper bound that takes the joint error into account. Then we further pursue a tighter bound with reasonable constraints on the hypothesis space. Additionally, we adopt a novel cross domain discrepancy for dissimilarity measurement which alleviates the instability during adversarial learning. Extensive empirical evidence shows that an invariant representation is not enough to guarantee a good generalization performance in the target domain, as the joint error matters especially when the domain gap is huge. We believe our results take an important step towards understanding unsupervised domain adaptation, and also stimulate future work on the design of stronger adaptation algorithms that manage to align conditional distributions without using pseudo-labels from the target domain.

References

Peter L. Bartlett and Shahar Mendelson. Rademacher and gaussian complexities: Risk bounds and structural results. *J. Mach. Learn. Res.*, 3:463–482, 2002.

Shai Ben-David, John Blitzer, Koby Crammer, Alex Kulesza, Fernando Pereira, and Jennifer Vaughan. A theory of learning from different domains. *Machine Learning*, 79:151–175, 2010.

Konstantinos Bousmalis, Nathan Silberman, David Dohan, Dumitru Erhan, and Dilip Krishnan. Unsupervised pixel-level domain adaptation with generative adversarial networks. In *IEEE/CVF Conference on Computer Vision and Pattern Recognition*, pp. 95–104, 2017.

Jun Deng, Wei Dong, Richard Socher, Li-Jia Li, Kuntai Li, and Li Fei-Fei. Imagenet: A large-scale hierarchical image database. *IEEE Conference on Computer Vision and Pattern Recognition*, pp. 248–255, 2009.

Kamran Ghasedi Dizaji, Amirhossein Herandi, Cheng Deng, Weidong Cai, and Heng Huang. Deep clustering via joint convolutional autoencoder embed- ding and relative entropy minimization. In *International Conference on Computer Vision*, 2017.

Yaroslav Ganin and Victor Lempitsky. Unsupervised domain adaptation by backpropagation. In *Proceedings of the 32nd International Conference on Machine Learning*, volume 37, pp. 1180–1189. JMLR.org, 2015.

Yaroslav Ganin, Evgeniya Ustinova, Hana Ajakan, Pascal Germain, Hugo Larochelle, François Laviolette, Mario Marchand, and Victor Lempitsky. Domain-adversarial training of neural networks. *Journal of Machine Learning Research*, 17(1):2096–2030, 2016.

Muhammad Ghifary, W. Bastiaan Kleijn, Mengjie Zhang, David Balduzzi, and Wen Li. Deep reconstruction-classification networks for unsupervised domain adaptation. In *European Conference on Computer Vision*, volume 9908, pp. 597 – 613. Springer, 2016.

Ian Goodfellow, Jean Pouget-Abadie, Mehdi Mirza, Bing Xu, David Warde-Farley, Sherjil Ozair, Aaron Courville, and Yoshua Bengio. Generative adversarial nets. In *Advances in Neural Information Processing Systems*, pp. 2672–2680. Curran Associates, Inc., 2014.

Kaiming He, Xiangyu Zhang, Shaoqing Ren, and Jian Sun. Deep residual learning for image recognition. *IEEE Conference on Computer Vision and Pattern Recognition*, pp. 770–778, 2015.

Judy Hoffman, Eric Tzeng, Taesung Park, Jun-Yan Zhu, Phillip Isola, Kate Saenko, Alexei Efros, and Trevor Darrell. CyCADA: Cycle-consistent adversarial domain adaptation. In *Proceedings of the 35th International Conference on Machine Learning*, volume 80, pp. 1989–1998. PMLR, 2018.

Jonathan Hull. Database for handwritten text recognition research. *IEEE Transactions on Pattern Analysis and Machine Intelligence*, 16:550 – 554, 1994.

Ying Jin, Ximei Wang, Mingsheng Long, and Jianmin Wang. Minimum class confusion for versatile domain adaptation. In *European Conference on Computer Vision*, 2020.

Minyoung Kim, Pritish Sahu, Behnam Gholami, and Vladimir Pavlovic. Unsupervised visual domain adaptation: A deep max-margin gaussian process approach. In *IEEE Conference on Computer Vision and Pattern Recognition*, 2019.

Diederik P. Kingma and Jimmy Ba. Adam: A method for stochastic optimization. *CoRR*, abs/1412.6980, 2014.

V. Koltchinskii and D. Panchenko. Empirical margin distributions and bounding the generalization error of combined classifiers. *Ann. Statist.*, 30(1):1–50, 2002.

Vladimir Koltchinskii and Dmitriy Panchenko. Rademacher processes and bounding the risk of function learning. In *High Dimensional Probability II*, pp. 443–457. Birkhäuser Boston, 2000.

Alex Krizhevsky, Ilya Sutskever, and Geoffrey E Hinton. Imagenet classification with deep convolutional neural networks. In *Advances in Neural Information Processing Systems*, pp. 1097–1105. Curran Associates, Inc., 2012.

Yann LeCun, Léon Bottou, Yoshua Bengio, and Patrick Haffner. Gradient-based learning applied to document recognition. In *Proceedings of the IEEE*, volume 86, pp. 2278–2324, 1998.

Dong-Hyun Lee. Pseudo-label : The simple and efficient semi-supervised learning method for deep neural networks. *ICML 2013 Workshop on Challenges in Representation Learning*, 2013.

Yanghao Li, Naiyan Wang, Jianping Shi, Xiaodi Hou, and Jiaying Liu. Adaptive batch normalization for practical domain adaptation. *Pattern Recognition*, 80:109–117, 2018.

Tsung-Yi Lin, Michael Maire, Serge J. Belongie, Lubomir D. Bourdev, Ross B. Girshick, James Hays, Pietro Perona, Deva Ramanan, Piotr Dollár, and C. Lawrence Zitnick. Microsoft coco: Common objects in context. In *European Conference on Computer Vision*, 2014.

Ming-Yu Liu and Oncel Tuzel. Coupled generative adversarial networks. In *Advances in Neural Information Processing Systems*, pp. 469–477. Curran Associates, Inc., 2016.

Mingsheng Long, Jianmin Wang, Guiguang Ding, Jia-Guang Sun, and Philip S. Yu. Transfer feature learning with joint distribution adaptation. *IEEE International Conference on Computer Vision*, pp. 2200–2207, 2013.

Mingsheng Long, Yue Cao, Jianmin Wang, and Michael I. Jordan. Learning transferable features with deep adaptation networks. In *Proceedings of the 32nd International Conference on International Conference on Machine Learning*, volume 37, pp. 97–105. JMLR.org, 2015.

Mingsheng Long, Han Zhu, Jianmin Wang, and Michael I. Jordan. Deep transfer learning with joint adaptation networks. In *Proceedings of the 34th International Conference on Machine Learning*, volume 70, pp. 2208–2217. JMLR.org, 2017.

Mingsheng Long, ZHANGJIE CAO, Jianmin Wang, and Michael I Jordan. Conditional adversarial domain adaptation. In *Advances in Neural Information Processing Systems*, pp. 1640–1650. Curran Associates, Inc., 2018.

Yishay Mansour, Mehryar Mohri, and Afshin Rostamizadeh. Domain adaptation: Learning bounds and algorithms. In *COLT*, 2009.

Mehdi Mirza and Simon Osindero. Conditional generative adversarial nets, 2014.

Takeru Miyato, Toshiki Kataoka, Masanori Koyama, and Yuichi Yoshida. Spectral normalization for generative adversarial networks. *ArXiv*, abs/1802.05957, 2018.

Zak Murez, Soheil Kolouri, David J. Kriegman, Ravi Ramamoorthi, and Kyungnam Kim. Image to image translation for domain adaptation. *IEEE/CVF Conference on Computer Vision and Pattern Recognition*, pp. 4500–4509, 2017.

Yuval Netzer, Tao Wang, Adam Coates, Alessandro Bissacco, Bo Wu, and Andrew Y. Ng. Reading digits in natural images with unsupervised feature learning. In *NIPS Workshop on Deep Learning and Unsupervised Feature Learning*, 2011.

S J Pan, I W Tsang, J T Kwok, and Q Yang. Domain adaptation via transfer component analysis. *IEEE Transactions on Neural Networks*, 22(2):199–210, 2011.

Sinno Jialin Pan, Ivor Wai-Hung Tsang, James T. Kwok, and Qiang Yang. Domain adaptation via transfer component analysis. *IEEE Transactions on Neural Networks*, 22:199–210, 2009.

Xingchao Peng, Ben Usman, Neela Kaushik, Judy Hoffman, Dequan Wang, and Kate Saenko. Visda: The visual domain adaptation challenge. *ArXiv*, abs/1710.06924, 2017.

Kate Saenko, Brian Kulis, Mario Fritz, and Trevor Darrell. Adapting visual category models to new domains. In *European Conference on Computer Vision*, pp. 213–226. Springer-Verlag, 2010.

Kuniaki Saito, Yoshitaka Ushiku, and Tatsuya Harada. Asymmetric tri-training for unsupervised domain adaptation. In *Proceedings of the 34th International Conference on Machine Learning*, volume 70, pp. 2988–2997. PMLR, 2017a.

Kuniaki Saito, Kohei Watanabe, Yoshitaka Ushiku, and Tatsuya Harada. Maximum classifier discrepancy for unsupervised domain adaptation. *IEEE/CVF Conference on Computer Vision and Pattern Recognition*, pp. 3723–3732, 2017b.

Swami Sankaranarayanan, Yogesh Balaji, Carlos D. Castillo, and Rama Chellappa. Generate to adapt: Aligning domains using generative adversarial networks. *CoRR*, abs/1704.01705, 2017.

Ozan Sener, Hyun Oh Song, Ashutosh Saxena, and Silvio Savarese. Learning transferrable representations for unsupervised domain adaptation. In *Advances in Neural Information Processing Systems*, pp. 2110–2118. Curran Associates, Inc., 2016.

Ashish Shrivastava, Tomas Pfister, Oncel Tuzel, Josh Susskind, Wenda Wang, and Russell Webb. Learning from simulated and unsupervised images through adversarial training. *IEEE Conference on Computer Vision and Pattern Recognition*, pp. 2242–2251, 2016.

Hui Tang, Ke Chen Chen, and Kui Jia. Unsupervised domain adaptation via structurally regularized deep clustering. In *IEEE Conference on Computer Vision and Pattern Recognition*, 2020.

Eric Tzeng, Judy Hoffman, Kate Saenko, and Trevor Darrell. Adversarial discriminative domain adaptation. *IEEE Conference on Computer Vision and Pattern Recognition*, pp. 2962–2971, 2017.

Laurens van der Maaten and Geoffrey Hinton. Visualizing data using t-SNE. *Journal of Machine Learning Research*, 9:2579–2605, 2008.

Hemanth Venkateswara, Jose Eusebio, Shayok Chakraborty, and Sethuraman Panchanathan. Deep hashing network for unsupervised domain adaptation. *IEEE Conference on Computer Vision and Pattern Recognition*, pp. 5385–5394, 2017.

Hui Wang, Jian Tian, Songyuan Li, Hanbin Zhao, Qi Tian, Fei Wu, and Xi Li. Structure-conditioned adversarial learning for unsupervised domain adaptation. volume 497, pp. 216–229, 2022.

Qian Wang and Toby P. Breckon. Unsupervised domain adaptation via structured prediction based selective pseudo-labeling. In *AAAI Conference on Artificial Intelligence*, 2020.

Yifan Wu, Ezra Winston, Divyansh Kaushik, and Zachary Lipton. Domain adaptation with asymmetrically-relaxed distribution alignment. volume 97 of *Proceedings of Machine Learning Research*, pp. 6872–6881. PMLR, 2019.

Jianfei Yang, Han Zou, Yuxun Zhou, Zhaoyang Zeng, and Lihua Xie. Mind the discriminability: Asymmetric adversarial domain adaptation. In *European Conference on Computer Vision*, 2020.

Weichen Zhang, Wanli Ouyang, Wen Li, and Dong Xu. Collaborative and adversarial network for unsupervised domain adaptation. *IEEE/CVF Conference on Computer Vision and Pattern Recognition*, pp. 3801–3809, 2018.

Yabin Zhang, Hui Tang, Kui Jia, and Mingkui Tan. Domain-symmetric networks for adversarial domain adaptation. In *IEEE Conference on Computer Vision and Pattern Recognition*, 2019a.

Yuchen Zhang, Tianle Liu, Mingsheng Long, and Michael Jordan. Bridging theory and algorithm for domain adaptation. In *Proceedings of the 36th International Conference on Machine Learning*, volume 97, pp. 7404–7413. PMLR, 2019b.

Han Zhao, Remi Tachet Des Combes, Kun Zhang, and Geoffrey Gordon. On learning invariant representations for domain adaptation. volume 97 of *Proceedings of Machine Learning Research*, pp. 7523–7532. PMLR, 2019.

A Appendix

A.1 Experimental Setting

A.1.1 Digits Dataset

SVHN ↔ MNIST We firstly examine the adaptation from SVHN (Fig. 8a) to MNIST (Fig. 8b). We use the standard training set and testing set for both source and target domains. The feature extractor contains three 5×5 convolutional layers with stride two 3×3 max pooling placed after the first two convolutional layers and a single fully-connected layer. For classifiers, we use 2-layer fully-connected networks.

MNIST ↔ USPS As for the adaptation between MNIST and USPS (Fig. 8c), we follow the training protocol established in Long et al. (2013) by sampling 2000 images from MNIST and 1800 from USPS. As for the test samples , the standard version is used for both source and target domains. The feature generator contains two 5×5 convolutional layers with stride two 2×2 max pooling placed after each convolutional layer and a single fully-connected layer. For classifiers, we use 2-layer fully-connected networks.

Throughout the experiment, we employ the CNN architecture used in Saito et al. (2017b), where batch normalization is applied to each layer and a 0.5 rate of dropout is used between fully connected layers. Besides, spectral normalization (Miyato et al., 2018) is deployed for the classifiers in all of the following experiments to stabilize adversarial learning. The major reason we utilize this technique is because we observe a performance drop when the network is over-trained (it usually occurs after several hundreds epochs). We are still not sure whether it is caused by a over-fitting on the source error or a general neural network training problem related to early stop (this phenomenon can also be observed in other algorithms). One common solution is to use a gradient reversal layer(Ganin et al., 2016) to balance the weight between the source error and the discrepancy between the two domains. However, it will introduce more hyper-parameters to tune. Besides, in our proposed cross margin discrepancy, as is illustrated in Fig. 9, we maximize $\log f_1(x, y_1) + \log(1 - f_2(x, y_1))$ w.r.t the classifiers but minimize only $\log(1 - f_2(x, y_1))$ (a part of the objective) w.r.t the feature extractor to avoid unnecessary oscillation during adversarial learning. This implies the objective we try to maximize is not equivalent to that we try to minimize. And in such case, it is difficult to employ gradient reversal layer which is supposed to train the classifiers and the feature extractor in a single objective simultaneously. With the help of spectral normalization, we can ensure the classifiers is approximately Lipschitz such that the performance drop at an early stage can be avoided since the gradient w.r.t the classifiers will be relatively small. Adam (Kingma & Ba, 2014) is used for optimization with a mini-batch size of 128 and a learning rate of 10^{-4}. As for the SHS proposal, we verify the sensitivity of our model on various value for $\gamma = \{0.1, 0.5, 0.9, 1.0\}$. As for the THS proposal, setting $\eta = 0$ usually provides a reliable performance and the adaptation result changes subtly for different η.

(a) SVHN (b) MNIST (c) USPS

Figure 8: Random samples from each dataset.

A.1.2 VisDA Dataset

We further evaluate our method on object classification. The VisDA dataset (Peng et al., 2017) is used here, which is designed for 12-class adaptation task from synthetic object to real object images. Source domain contains 152,397 synthetic images, which are generated by rendering 3D CAD models. Data of the target domain is collected from MSCOCO (Lin et al., 2014) consisting of 55,388 real images. Since the 3D models are generated without the background and color diversity, the synthetic domain is quite different from the real domain, which makes it a much more difficult problem than digits adaptation. Again, this experiment

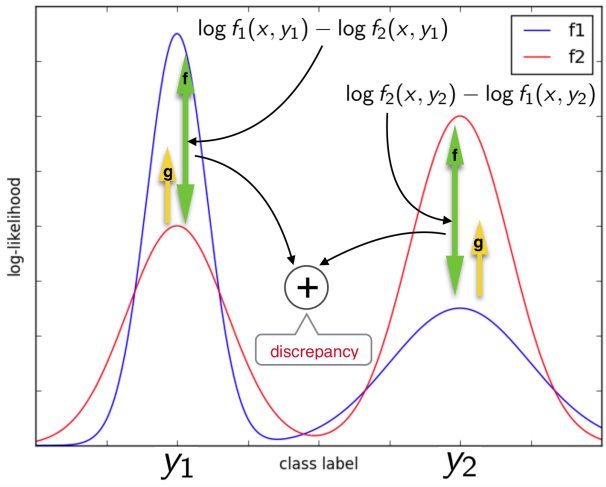

Figure 9: Illustrated details for the cross margin discrepancy

is performed in unsupervised fashion and no data augmentation technique excluding horizontal flipping is allowed.

Following the protocol established in Saito et al. (2017b), we evaluate our method by fine-tuning a ResNet-101 (He et al., 2015) model pretrained on ImageNet (Deng et al., 2009). The model except the last layer combined with a single-layer bottleneck is used as feature extractor and a randomly initialized 2-layer fully-connected network is used as a classifier, where batch normalization is applied to each layer and a 0.5 rate of dropout is conducted. Nesterov accelerated gradient is used for optimization with a mini-batch size of 32 and an initial learning rate of 10^{-3} which decays exponentially. The network architecture used in Saito et al. (2017b) is originally a 3-layer fully-connected classifier. However, as is mentioned in the main paper, we show that a relatively weaker classifier will improve the stability of the adversarial learning. Therefore, we take advantage of the framework proposed in Zhang et al. (2019b) by regarding the top layer of the classifier, i.e., a bottleneck, as a part of the feature extractor (it does not change the entire complexity of the model). Another crucial point here is that the network parameters w.r.t. the ResNet-101 and the bottleneck are updated separately at a ratio of 1:10, which is the same with Zhang et al. (2019b). A similar trick is used in Saito et al. (2017b) to relatively slow down the updating for ResNet-101 by introducing a Nesterov optimizer with a momentum term for the classifier. The common reason here that we do not want the feature extractor to be updated too much is very simple as ResNet-101 is so powerful that it can easily over-fit the source risk. We apply horizontal flipping of input images during training as the only data augmentation. As for the hyper-parameter, we test for $\gamma = \{0.1, 0.5, 0.9, 1\}$ and $\eta = \{0, 0.5, 0.8, 0.9\}$. For a direct comparison, we report the accuracy after 10 epochs.

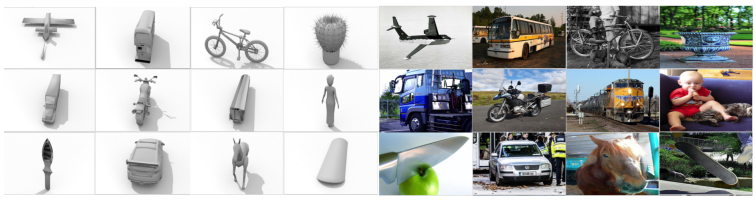

(a) synthetic images (b) real images

Figure 10: (a) Samples from source domain. (b) Samples from target domain.

A.1.3 Office-Home Dataset

Office-Home (Venkateswara et al., 2017) is a complex dataset (Fig. 11) containing 15,500 images from four significantly different domains: Art (paintings, sketches and/or artistic depictions), Clipart (clip art images), Product (images without background), and Real-world (regular images captured with a camera). In this experiment, following the protocol from Zhang et al. (2019b), we evaluate our method by fine-tuning a ResNet-50 (He et al., 2015) model pretrained on ImageNet (Deng et al., 2009). The model except the last layer combined with a single-layer bottleneck is used as feature extractor and a randomly initialized 2-layer fully-connected network with width 1024 is used as a classifier, where batch normalization is applied to each layer and a 0.5 rate of dropout is conducted. For optimization, we use the SGD with the Nesterov momentum term fixed to 0.9, where the batch size is 32 and learning rate is adjusted according to Ganin et al. (2016).We apply horizontal flipping and resized cropping of input images during training as the data augmentation similar to Zhang et al. (2019b).

Here we introduce a slightly different loss for $\tilde{\epsilon}_{T_g}(f_2)$. For the unlabeled target data $\{x_t^i \in T\}_{i=1}^m$, the network predictions given by h, f_2 are represented with $\{q_i \in Q\}_{i=1}^m$ and $\{p_i \in P\}_{i=1}^m$ where the confidence towards class k is defined by:

$$q_{i,k} = h(g(x_t^i), y = k), \quad p_{i,k} = f_2(g(x_t^i), y = k)$$

In addition to the hypothesis space constraint, we add a class balance regularization term for f_2 to encourage entropy maximization of the label distribution on the target domain, which improves the performance especially when the class number is large(Saito et al., 2017b):

$$\min_p \frac{1}{m} \sum_{i=1}^m KL(p_i || q_i) + \sum_{k=1}^K \frac{\sum_{i=1}^m p_{i,k}}{m} \log \frac{\sum_{i=1}^m p_{i,k}}{m}$$

For fixed Q, by setting the approximate gradient as zero, we has the following closed-form solution for the above problem(Dizaji et al., 2017):

$$p_{i,k}^* = \frac{q_{i,k}/\sqrt{\sum_{i=1}^m q_{i,k}}}{\sum_{k=1}^K q_{i,k}/\sqrt{\sum_{i=1}^m q_{i,k}}}$$

Finally, we train g, f_2 to push $p_{i,k}$ towards $p_{i,k}^*$ by minimizing the following KL divergence:

$$\tilde{\epsilon}_{T_g}(f_2) = -\frac{1}{m} \sum_{i=1}^m \sum_{k=1}^K p_{i,k}^* \log f_2(g(x_t^i), y = k) \tag{9}$$

Figure 11: Sample images from the Office-Home dataset (Venkateswara et al., 2017).

A.1.4 Office-31 Dataset

Office-31 (Saenko et al., 2010) (Fig. 12) is a popular dataset to verify the effectiveness of a domain adaptation algorithm, which contains three diverse domains, Amazon from Amazon website, Webcam by web camera

and DSLR by digital SLR camera with 4,652 images in 31 unbalanced classes. Besides, we show several noisy samples in Fig.13 to backup our assumption for the failure case. In this experiment, following the protocol from Zhang et al. (2019b), we evaluate our method by fine-tuning a ResNet-50 (He et al., 2015) model pretrained on ImageNet (Deng et al., 2009). The model used here is almost identical to the one in Office-Home experiment except a different width 2048 for classifiers. For optimization, we use the SGD with the Nesterov momentum term fixed to 0.9, where the batch size is 32 and learning rate is adjusted according to Ganin et al. (2016). We apply horizontal flipping and resized cropping of input images during training as the data augmentation similar to Zhang et al. (2019b).

Figure 12: Sample images from the Office-31 dataset.

Figure 13: Noisy images from the Office-31 dataset.

A.2 Comparisons with Other Methods

In this section, we show that under some conditions, the proposed joint error based upper bound can reduce to other popular upper bounds, which demonstrates the generality of our proposal.

A.2.1 Margin Disparity Discrepancy

Zhang et al. (2019b) propose a novel margin-aware generalization bound based on scoring functions and define a new divergence MDD. The training objective used in MDD can be alternatively expressed as (here $\epsilon(h, f)$ denotes the margin disparity):

$$\min_{g \in H_g, h \in H_f} [\epsilon_{S_g}(h) + \max_{f \in H_f} (\epsilon_{T_g}(f, h) - \epsilon_{S_g}(f, h))]$$

Recall Eq.3, if we set $f_1 = f_2 = f$ and free the constraint of f to any $f \in H_f$, our proposal degrades exactly to MDD. As discussed above, the assumption about identical optimal labeling function $f_S = f_T$ is dangerous, because we have no idea about the location of f_T and a perfect alignment between the conditional distributions of source and target domain is not likely to happen in practice. Besides, an unconstrained hypothesis space for f is not helpful to build a tight bound.

A.2.2 Maximum Classifier Discrepancy

Saito et al. (2017b) propose two task-specific classifiers f_1, f_2 that are used to separate the decision boundary on the source domain, such that the feature extractor is encouraged to produce features near the support of

the source samples. The objective used in MCD can be alternatively expressed as:

$$\begin{cases} \min_{g \in H_g}[\epsilon_{S_g}(f_1) + \max_{f_1 \in H, f_2 \in H}(\epsilon_{T_g}(f_1, f_2))] \\ \text{s.t.} \quad H = \{f | \arg\min_{f \in H_f, g \in H_g} \epsilon_{S_g}(f)\} \end{cases}$$

Recall Eq.3, if we set $\gamma = \eta = 1$ and $h = f_1$, our proposal reduces to MCD. As proved in 3.1, the proposed upper bound is optimized when $h = f_S$. However, it no longer holds after the upper bound is relaxed by taking the supremum, i.e., setting $h = f_1$ does not necessarily minimize the objective. Besides, as discussed above, assuming $H_2 = H_{sc} = H_1$ lacks generality since f_T can be far away from f_S and does not necessarily classify all source samples, which means the assumption of MCD is not likely to be applicable to those cases where a huge domain gap exists.

A.3 Rademacher Complexity

Let H be a set of real-valued functions defined over a set X. Given a sample $S \in X^m$, the empirical Rademacher complexity of H is defined as follows:

$$\hat{\Re}_S(H) = \frac{2}{m}\mathbb{E}_\sigma \left[\sup_{h \in H} |\sum_{i=1}^{m} \sigma_i h(x_i)| \middle| S = (x_1, ..., x_m) \right]$$

The expectation is taken over $\sigma = (\sigma_1, ..., \sigma_n)$ where σ_i is an independent uniform random variable taking values in $\{-1, +1\}$.

The Rademacher complexity measures the ability of a class of functions to fit noise and also has the additional advantage that it is data-dependent and can be measured from finite samples, which can lead to tighter bounds than those based on other measures of complexity such as the VC-dimension. Following the established theory proposed by Mansour et al. (2009), we denote the empirical average of a hypothesis $h : X \to \{0, 1\}$ by $\hat{R}(h)$ and its expectation over samples drawn according to the distribution considered by $R(h)$. The following gives a version of the Rademacher complexity bounds (Koltchinskii & Panchenko, 2000; Bartlett & Mendelson, 2002):

Let H be a class of functions mapping $X \times Y \to [0, 1]$ and $S = ((x_1, y_1), ..., (x_m, y_m))$ a finite sample drawn i.i.d. according to a distribution Q. Then, for any $\sigma > 0$, with probability at least $1 - \sigma$ over samples S of size m, the following inequality holds for all $h \in H$:

$$R(h) \leq \hat{R}(h) + \hat{\Re}_S(H) + 3\sqrt{\frac{\log \frac{2}{\sigma}}{2m}}$$

Recall our proposed upper bound, we have: $\epsilon_T(h) \leq \epsilon_S(h) + C_{S,T}(f_S, f_T, h)$ where $C_{S,T}$ is further bounded by: $\sup_{f_1 \in H_1, f_2 \in H_2}\{\epsilon_T(f_1, f_2) + \epsilon_S(f_1, f_2) + \epsilon_T(h, f_1) - \epsilon_S(h, f_2)\}$. Now we relax this bound by applying $\epsilon_S(f_1, f_2) \leq \epsilon_S(f_1, h) + \epsilon_S(f_2, h)$ and name it $d(S, T; h) = \sup_{f_1 \in H_1, f_2 \in H_2}\{\epsilon_T(f_1, f_2) + \epsilon_S(f_1, h) + \epsilon_T(f_1, h)\}$. Assume that the loss function ϵ is bounded by $M > 0$:$\epsilon(h, h') \leq M$ for all $h, h' \in H$. Let Q be a distribution over X and let $\hat{Q}$ denote the corresponding empirical distribution for a sample $S = (x_1, ..., x_m)$. Then we can scale the loss ϵ to $[0, 1]$ by dividing by M, and denote the new class by ϵ_{H_1,H_2} which represents the class of functions $\{x \to \epsilon(f_1(x), f_2(x)) : f_1 \in H_1, f_2 \in H_2\}$. By the above theorem , for any $\sigma > 0$, with probability at least $1 - \sigma$, the following inequality holds for all $f_1 \in H_1, f_2 \in H_2$:

$$\frac{\epsilon_Q(f_1, f_2)}{M} \leq \frac{\epsilon_{\hat{Q}}(f_1, f_2)}{M} + \hat{\Re}_S(\epsilon_{H_1,H_2}/M) + 3\sqrt{\frac{\log \frac{2}{\sigma}}{2m}}$$

The empirical Rademacher complexity has the property that $\hat{\Re}(\alpha H) = \alpha\hat{\Re}(H)$ for any hypothesis class H and positive number α, which helps simplify the above bound. Now let S be a distribution over X and $\hat{S}$ the corresponding empirical distribution for a sample $\tilde{S}$, and let T be a distribution over X and $\hat{T}$ the

corresponding empirical distribution for a sample $\tilde{T}$. Then, for any $\sigma > 0$, with probability at least $1 - \sigma$ over samples $\tilde{S}$ of size m drawn according to S and samples $\tilde{T}$ of size n drawn according to T, we can write:

$$\begin{aligned} d(S,T;h) \leq & \sup_{f_1 \in H_1, f_2 \in H_2} \{\epsilon_{\hat{T}}(f_1,f_2) + \epsilon_{\hat{S}}(f_1,h) + \epsilon_{\hat{T}}(f_1,h)\} \\ & + \hat{\Re}_{\tilde{T}}(\epsilon_{H_1,H_2}) + \hat{\Re}_{\tilde{S}}(\epsilon_{H_1}) + \hat{\Re}_{\tilde{T}}(\epsilon_{H_1}) \\ & + 3M(\sqrt{\frac{\log\frac{2}{\sigma}}{2m}} + 2\sqrt{\frac{\log\frac{2}{\sigma}}{2n}}) \end{aligned}$$

A.4 Compatibility

We do agree that it is not easy to find the true labeling function inside a specific hypothesis space. However, we believe it is a feasible assumption that labeling functions lie in a hypothesis space with enough complexity. For instance, Mansour et al. (2009) makes a similar assumption that H includes f_T. Besides, since the algorithm is always run within finite samples, there is quite likely to be a function inside a specific hypothesis space that could perfectly mimic the behavior of the true labeling function on those samples. Therefore, even if the hypothesis space we use does not contain the true labeling function, it will not harm the actual learning process. The proof is as below:

$$\begin{aligned} \epsilon_T(h) &= \epsilon_T(h, f_T) \\ &= \epsilon_T(h,f_T) - \epsilon_T(h,f_S) + \epsilon_T(h,f_S) + \epsilon_S(h,f_S) - \epsilon_S(h,f_S) + \epsilon_S(h,f_T) - \epsilon_S(h,f_T) \\ &= \epsilon_S(h,f_S) + (\epsilon_T(h,f_T) - \epsilon_T(h,f_S)) + (\epsilon_S(h,f_T) - \epsilon_S(h,f_S)) + \epsilon_T(h,f_S) - \epsilon_S(h,f_T) \\ &\leq \epsilon_S(h) + \epsilon_T(f_S,f_T) + \epsilon_S(f_S,f_T) + \epsilon_T(h,f_S) - \epsilon_S(h,f_T) \\ &\leq \epsilon_S(h) + \epsilon_T(f_S,f_S^*) + \epsilon_T(f_S^*,f_T^*) + \epsilon_T(f_T^*,f_T) + \epsilon_S(f_S,f_S^*) + \epsilon_S(f_S^*,f_T^*) + \epsilon_S(f_T^*,f_T) \\ &\quad + \epsilon_T(h,f_S^*) + \epsilon_T(f_S^*,f_S) - \epsilon_S(h,f_T^*) + \epsilon_S(f_T^*,f_T) \\ &= \epsilon_S(h) + C_{S,T}(f_S^*,f_T^*,h) + \theta \end{aligned}$$

where $\theta = 2\epsilon_T(f_S,f_S^*) + \epsilon_S(f_S,f_S^*) + 2\epsilon_S(f_T^*,f_T) + \epsilon_T(f_T^*,f_T)$.

We assume $f_S^* = \arg\min_{f\in H} \epsilon_{S\bigcup 2T}(f_S,f)$ and $f_T^* = \arg\min_{f\in H} \epsilon_{2S\bigcup T}(f_T,f)$. If $f_S^*, f_T^* \in H$ can perfectly mimic the behavior of f_S, f_T on S and T, then θ can be totally ignored and the obtained bound become compatible with the original upper bound by replacing f_S, f_T with f_S^*, f_T^*.

A.5 Validity

In Sec.3.2, we make the following assumption that it is possible to build two subspaces $H_1, H_2 \subseteq H_f$ such that:

$$C_{S_g,T_g}(f_S,f_T,h) \leq \max_{f_1\in H_1, f_2\in H_2} C_{S_g,T_g}(f_1,f_2,h)$$

The assumption is hard to prove theoretically, thus we show the validity of the inequality by experimental results instead. In this section, we choose an adaptation scenario where the domain gap is large (Product to Clipart scenarion of Office-Home dataset). We use the full source and target labels to estimate $C_{S_g,T_g}(f_S,f_T,h)$ as the ground truth. The upper bound is computed with two subspaces H_1, H_2 given by target-driven hypothesis space proposal (Sec.3.2.1) that utilizes pseudo labels:

$$H_1 = \{f_1 | \arg\min_{f_1\in H_f, g\in H_g} \epsilon_{S_g}(f_1)\}, \quad H_2 = \{f_2 | \arg\min_{f_2\in H_f, g\in H_g} \eta\epsilon_{S_g}(f_2) + (1-\eta)\tilde{\epsilon}_{T_g}(f_2)\}$$

Fig.14 demonstrates that our proposal remains a valid upper bound in practice even if the domain gap is so large that the subspace H_2 we built is not likely contains f_T.

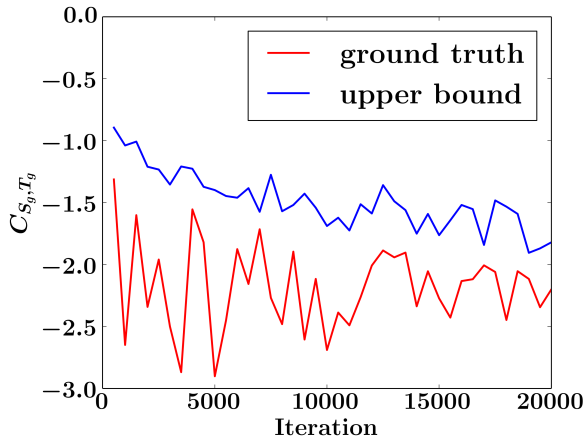

Figure 14: The estimated means of ground truth and upper bound by 3 runs in scenario Pr→Cl adapted with $THS + CMD$ proposal.

A.6 Proof

A.6.1 Proof for the Upper Bound

Given the above notations and triangle inequality, we have:

$$\begin{aligned}
\epsilon_T(h) &= \epsilon_T(h, f_T) \\
&= \epsilon_T(h, f_T) + [\epsilon_T(h, f_S) - \epsilon_T(h, f_S)] + [\epsilon_S(h, f_S) - \epsilon_S(h, f_S)] + [\epsilon_S(h, f_T) - \epsilon_S(h, f_T)] \\
&= \epsilon_S(h, f_S) + [\epsilon_T(h, f_T) - \epsilon_T(h, f_S)] + [\epsilon_S(h, f_T) - \epsilon_S(h, f_S)] + \epsilon_T(h, f_S) - \epsilon_S(h, f_T) \\
&\leq \epsilon_S(h) + \epsilon_T(f_S, f_T) + \epsilon_S(f_S, f_T) + \epsilon_T(h, f_S) - \epsilon_S(h, f_T)
\end{aligned}$$

A.6.2 Proof for the Optimum

We demonstrate our upper bound is minimized when $h = f_S$, and it is equivalent to $\epsilon_T(f_S, f_T)$.

Firstly, when we set $h = f_S$, we have:

$$\epsilon_S(h) + \epsilon_T(f_S, f_T) + \epsilon_S(f_S, f_T) + \epsilon_T(h, f_S) - \epsilon_S(h, f_T) = \epsilon_T(f_S, f_T)$$

Then, according to the triangle inequality and non-negativity of a distance metric, we have:

$$\begin{aligned}
&[\epsilon_S(h) + \epsilon_S(f_S, f_T)] + \epsilon_T(f_S, f_T) + \epsilon_T(h, f_S) - \epsilon_S(h, f_T) \\
&\qquad \geq \epsilon_S(h, f_T) + \epsilon_T(f_S, f_T) + \epsilon_T(h, f_S) - \epsilon_S(h, f_T) \\
&\qquad = \epsilon_T(f_S, f_T) + \epsilon_T(h, f_S) \\
&\qquad \geq \epsilon_T(f_S, f_T)
\end{aligned}$$

A.6.3 Proof for the Relation to Joint error

We demonstrate when our upper bound is minimized, it is equivalent to an upper bound of optimal joint error λ because:

$$\begin{aligned}
\epsilon_T(f_S, f_T) &= \epsilon_T(f_S, f_T) + \epsilon_S(f_S, f_S) \\
&= \epsilon_T(f_S) + \epsilon_S(f_S) \\
&\geq \min_{h \in H}(\epsilon_T(h) + \epsilon_S(h)) = \lambda
\end{aligned}$$

A.7 Hyperparameter Selection

In all experiments, the hyper-parameters γ, η are set based on the validation performance on a separate dataset consisting of a few hundreds of labeled target samples. As showed in the main paper, it can be seen that the performance of our proposal is quite sensitive to the change of the hyper-parameters. However, it also suggests that an appropriate choice of the hyper-parameters can significantly boost the performance, which allows us to select the hyper-parameters via a validation dataset with 200 samples. Fig. 15 shows two examples of the validation performance on different adaptation tasks w.r.t. γ, η.

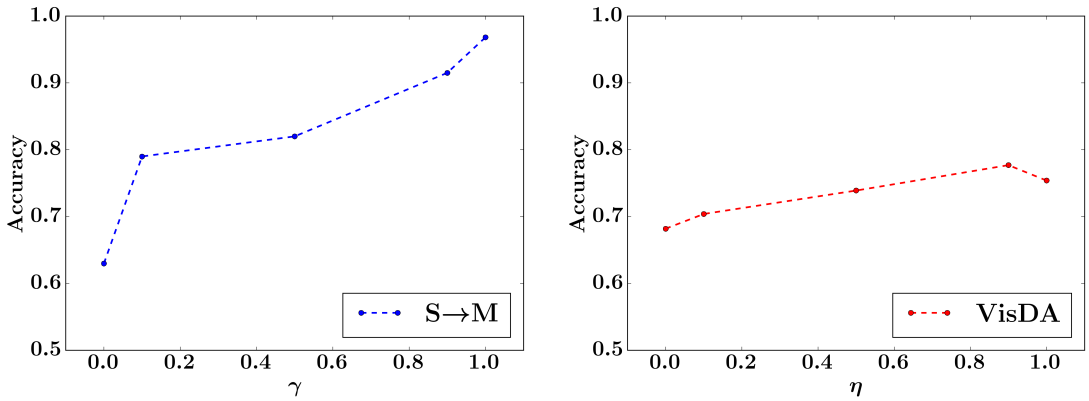

(a) $THS + L_1$ where $\eta = 1$

(b) $THS + CMD$ where $\gamma = \eta$

Figure 15: Validation performance when varying the hyper-parameters γ, η on a separate dataset

A.8 Relations between the Margin Theory and CMD

The margin between data points and the classification surface plays a significant role in achieving strong generalization performance. In order to quantify ϵ into a differentiable measurement as a surrogate of 0-1 loss, we introduce the margin theory developed by Koltchinskii & Panchenko (2002), where the margin loss is interpreted as:

$$\mathbb{E}_{(x,y)\in D}[\max(0, 1 + \max_{y' \neq y} s(y'|x) - s(y|x))]$$

where the output of a score function $s(y|x)$ for multi-class classification indicates the confidence of the prediction on class y.

We aim to utilize this concept to further improve the reliability of our proposed method by leveraging this margin loss to define a novel measurement of the discrepancy between two hypotheses f_1, f_2 (e.g., a multi-layer perceptron whose output layer is a softmax function) over a distribution D, namely cross margin discrepancy:

$$\epsilon_D(f_1, f_2) = \mathbb{E}_{x\in D}[\mathrm{cmd}(f_1, f_2; x)]$$

Before further discussion, we firstly introduce two distributions D_{f_1}, D_{f_2}induced by labeling functions f_1, f_2 respectively, where $D_{f_1} = \{(x, l_{f_1}(x))|x \sim D\}$ and $D_{f_2} = \{(x, l_{f_2}(x))|x \sim D\}$ (function l returns the predictive labels). Then we consider the case where two hypotheses (f_1, f_2) disagree, i.e., $y_1 = l_{f_1}(x) \neq l_{f_2}(x) = y_2$, and the primitive loss is defined as:

$$\begin{aligned}\mathrm{cmd}(f_1, f_2; x) &= \log f_1(y_1|x) - \log f_2(y_1|x) + \log f_2(y_2|x) - \log f_1(y_2|x) \\ &= \log f_1(y_1|x) - \log f_1(y_2|x) + \log f_2(y_2|x) - \log f_2(y_1|x)\end{aligned}$$

Then the cross margin discrepancy $\epsilon_D(f_1, f_2)$ can be viewed as:

$$\mathbb{E}_{(x,y)\in D_{f_2}}[\max_{y'\neq y} \log f_1(y'|x) - \log f_1(y|x)] + \mathbb{E}_{(x,y)\in D_{f_1}}[\max_{y'\neq y} \log f_2(y'|x) - \log f_2(y|x)]$$

which is a sum of the margin loss for f_1 on D_{f_2} and the margin loss for f_2 on D_{f_1}, if we use the logarithm of softmax as the score function.

Thanks to the trick introduced by Goodfellow et al. (2014) to mitigate the burden of exploding or vanishing gradients, we optimize a dual form of the above primitive loss in practice:

$$\text{cmd}(f_1, f_2; x) = \log f_1(y_1|x) + \log(1 - f_1(y_2|x)) + \log f_2(y_2|x) + \log(1 - f_2(y_1|x))$$

A.9 Details of the Training Objective

This section briefly explains the training objective of the proposed method. Here we take THS objective as an example and each term in the objective is clearly defined below:

$$\begin{cases} \min_{g\in H_g, h\in H_f}[\epsilon_{S_g}(h) + \max_{f_1\in H_1, f_2\in H_2} C_{S_g,T_g}(f_1, f_2, h)] \\ \text{s.t.} \quad H_1, H_2 = \{f_1, f_2 | \arg\min_{f_1,f_2\in H_f, g\in H_g}[\epsilon_{S_g}(f_1) + \gamma\epsilon_{S_g}(f_2) + (1-\eta)\tilde{\epsilon}_{T_g}(f_2)]\} \end{cases}$$

where g represent a feature extractor and h, f_1, f_2 are classifiers with a softmax output (i.e., $h(x, y)$ represents the confidence of sample x being classified as label y). First, we can use the cross-entropy loss to achieve the hypothesis space constraint:

$$\begin{cases} \epsilon_{S_g}(f_1) = -\mathbb{E}_{x,y\sim S} \log(f_1(y|g(x))) \\ \gamma\epsilon_{S_g}(f_2) + (1-\eta)\tilde{\epsilon}_{T_g}(f_2) = -\gamma\mathbb{E}_{x,y\sim S} \log(f_2(y|g(x))) - (1-\eta)\mathbb{E}_{x\sim T} \log(f_2(l_h(x)|g(x))) \end{cases}$$

Then we use the proposed cross margin discrepancy to reorganize $C_{S_g,T_g}(f_1, f_2, h)$. Before further derivation, we introduce three proxy distributions $S_{f_1=f_2}, S_{f_1\setminus f_2}, S_{f_2\setminus f_1}$ induced by f_1, f_2, where $S_{f_1=f_2} = \{x, y|x \sim S, l_{f_1}(x) = l_{f_2}(x) = y\}, S_{f_1\setminus f_2} = \{x, y|x \sim S, y = l_{f_1}(x) \neq l_{f_2}(x)\}, S_{f_2\setminus f_1} = \{x, y|x \sim S, l_{f_1}(x) \neq l_{f_2}(x) = y\}$ (the labeling function l returns labels of the most confident prediction by f). Analogously, we define others like $S_{f_1=h}, S_{f_2=h}, T_{f1\setminus f2}$, etc. According to the definition of CMD (Sec.3.3):

$$\begin{aligned}
&\hat{C}_{S_g,T_g}(f_1, f_2, h) \\
&= \mathbb{E}_{x,y\sim S_{f_1=f_2}}[\log\max(f_1(y|g(x)), f_2(y|g(x))) + \log\max(1 - f_1(y|g(x)), 1 - f_2(y|g(x)))] \\
&+ \mathbb{E}_{x,y\sim S_{f_1\setminus f_2}}[\log f_1(y|g(x)) + \log(1 - f_2(y|g(x)))] + \mathbb{E}_{x,y\sim S_{f_2\setminus f_1}}[\log(1 - f_1(y|g(x))) + \log f_2(y|g(x))] \\
&+ \mathbb{E}_{x,y\sim T_{f_1=f_2}}[\log\max(f_1(y|g(x)), f_2(y|g(x))) + \log\max(1 - f_1(y|g(x)), 1 - f_2(y|g(x)))] \\
&+ \mathbb{E}_{x,y\sim T_{f_1\setminus f_2}}[\log f_1(y|g(x)) + \log(1 - f_2(y|g(x)))] + \mathbb{E}_{x,y\sim T_{f_2\setminus f_1}}[\log(1 - f_1(y|g(x))) + \log f_2(y|g(x))] \\
&+ \mathbb{E}_{x,y\sim T_{f_1=h}}[\log\max(f_1(y|g(x)), h(y|g(x))) + \log\max(1 - f_1(y|g(x)), 1 - h(y|g(x)))] \\
&+ \mathbb{E}_{x,y\sim T_{f_1\setminus h}}[\log f_1(y|g(x)) + \log(1 - h(y|g(x)))] + \mathbb{E}_{x,y\sim T_{h\setminus f_1}}[\log(1 - f_1(y|g(x))) + \log h(y|g(x))] \\
&- \mathbb{E}_{x,y\sim S_{f_2=h}}[\log\max(h(y|g(x)), f_2(y|g(x))) + \log\max(1 - h(y|g(x)), 1 - f_2(y|g(x)))] \\
&- \mathbb{E}_{x,y\sim S_{f_2\setminus h}}[\log f_2(y|g(x)) + \log(1 - h(y|g(x)))] - \mathbb{E}_{x,y\sim S_{h\setminus f_2}}[\log(1 - f_2(y|g(x))) + \log h(y|g(x))]
\end{aligned} \tag{10}$$

where part of this objective can be regarded as a CGAN objective aiming to align the conditional distributions of three pairs of hypothesis induced distributions ($S_{f_1=f_2} \Leftrightarrow T_{f_1=f_2}$, $S_{f_1\setminus f_2} \Leftrightarrow T_{f_2\setminus f_1}$, $S_{f_2\setminus f_1} \Leftrightarrow T_{f_1\setminus f_2}$) under a minor assumption that f_1, f_2 are more confident about S, T respectively.

As we explain in A.1.1, in order to avoid unnecessary oscillation during adversarial learning, we only optimize a part of the objective (the part treated as fake by the classifier) w.r.t g, h so that it can be consistent with general GAN objective. This implies the objective ($\hat{C}_{S_g,T_g}(f_1, f_2, h)$) we try to maximize is not equivalent to

Table 5: Influence of λ on the adaptation of SVHN→MNIST under our proposal ($THS + CMD, \eta = 0$).

SVHN to MNIST	$\lambda = 0.001$	$\lambda = 0.01$	$\lambda = 0.1$
Acc	98.4±0.1	98.6±0.1	97.2±0.3

Table 6: The accuracy of ResNet-50 model fine-tuned on the Office-Home dataset. * represents the imbalance label distribution setting where we manually remove the samples of an entire class from the target domain.

METHOD	AR→CL	PR→CL	RW→CL
SOURCE ONLY	34.9	31.2	41.2
DANN(GANIN ET AL., 2016)	45.6	43.7	51.8
MCD(SAITO ET AL., 2017B)	51.9	51.6	55.8
CDAN(LONG ET AL., 2018)	50.7	50.9	56.7
SYMNETS(ZHANG ET AL., 2019A)	47.7	48.8	52.6
SPL(WANG & BRECKON, 2020)	54.5	53.1	55.3
AADA(YANG ET AL., 2020)	54.0	51.8	57.4
SRDC(TANG ET AL., 2020)	52.3	53.8	57.1
SCAL(WANG ET AL., 2022)	55.3	51.6	57.8
OURS ($THS + CMD, \eta = 0.9$)	60.3	59.2	62.7
DANN*	43.1	40.5	49.2
MCD*	50.5	49.7	54.3
OURS* ($THS + CMD, \eta = 0.9$)	60.0	58.5	62.2

that ($\check{C}_{S_g,T_g}(f_1, f_2, h)$) we try to minimize:

$$
\begin{aligned}
&\check{C}_{S_g,T_g}(f_1, f_2, h) \\
&= \mathbb{E}_{x,y\sim S_{f_1=f_2}} \log\max(1 - f_1(y|g(x)), 1 - f_2(y|g(x))) \\
&+ \mathbb{E}_{x,y\sim S_{f_1\setminus f_2}} \log(1 - f_2(y|g(x))) + \mathbb{E}_{x,y\sim S_{f_2\setminus f_1}} \log(1 - f_1(y|g(x))) \\
&+ \mathbb{E}_{x,y\sim T_{f_1=f_2}} \log\max(1 - f_1(y|g(x)), 1 - f_2(y|g(x))) \\
&+ \mathbb{E}_{x,y\sim T_{f_1\setminus f_2}} \log(1 - f_2(y|g(x))) + \mathbb{E}_{x,y\sim T_{f_2\setminus f_1}} \log(1 - f_1(y|g(x))) \\
&+ \mathbb{E}_{x,y\sim T_{f_1=h}} \log\max(1 - f_1(y|g(x)), 1 - h(y|g(x))) \\
&+ \mathbb{E}_{x,y\sim T_{f_1\setminus h}} \log(1 - h(y|g(x))) + \mathbb{E}_{x,y\sim T_{h\setminus f_1}} \log(1 - f_1(y|g(x))) \\
&- \mathbb{E}_{x,y\sim S_{f_2=h}} \log\max(1 - h(y|g(x)), 1 - f_2(y|g(x))) \\
&- \mathbb{E}_{x,y\sim S_{f_2\setminus h}} \log(1 - h(y|g(x))) - \mathbb{E}_{x,y\sim S_{h\setminus f_2}} \log(1 - f_2(y|g(x)))
\end{aligned} \tag{11}
$$

Since we apply different measurements to the source error and the discrepancy, we introduce a scaling factor λ to ensure that neither of them can dominate the back-propagation. $\lambda = 0.01$ is used in all experiments because we observe that source error is usually around $1e-2$ and the discrepancy is usually around $1e0$. We also conduct a simple experiment to check the influence of λ and report the results in Tab.5.

A.10 Imbalance Label Distribution

In this section, we conduct an additional experiment on the situation where the label distribution of source is very different from that of target domain. We choose Office-Home dataset and manually remove the samples of an entire class ('clock') from the target (Clipart) domain to create an imbalance scenario. We report the adaptation accuracy in Tab.6. In theory, our proposal does not suffer from the imbalance label distribution. Because unlike other methods that can only match the marginal distributions, our proposal is designed to align the conditional distributions. In practice, the experimental results demonstrate our theory since there is no remarkable performance drop in our proposal compared to other methods. Besides, despite this extreme imbalance label distribution case, our proposal still outperforms other methods that trained on the full target domain.

Table 7: A simple ablation study to reveal the contribution from each part of the proposal ($\surd$ in the column "optimal joint error" means to include the joint error in the upper bound, in contrast to the training objective proposed by MCD; $\surd$ in the column "cross margin discrepancy" means to use the proposed discrepancy measurement for ϵ, whereas $\times$ indicates we use L_1 norm instead; $\surd$ in the column "pseudo labels induced hypothesis space" means the hypothesis space for f_2 is built based on pseudo labels of target samples, which is corresponding to our THS proposal in the main paper where $\eta \neq 1$). We repeat the adaptation from SVHN to MNIST 5 times and report the average and the standard deviation of the accuracy.

METHOD	OPTIMAL JOINT ERROR	CROSS MARGIN DISCREPANCY	PSEUDO LABELS INDUCED HYPOTHESIS SPACE	SVHN TO MNIST
BASELINE	$\times$	$\times$	$\times$	96.2±0.4
	$\times$	$\surd$	$\times$	96.6±0.2
	$\times$	$\times$	$\surd$	97.1±0.3
	$\times$	$\surd$	$\surd$	97.6±0.2
OURS	$\surd$	$\times$	$\times$	96.8±0.2
	$\surd$	$\surd$	$\times$	97.5±0.2
	$\surd$	$\times$	$\surd$	98.2±0.2
	$\surd$	$\surd$	$\surd$	98.6±0.1

A.11 Ablation Study

In this section, we conduct a simple ablation study to show how each part of the proposal, i.e., the objective including the joint error, the cross margin discrepancy and the pseudo labels induced hypothesis space, contributes to the performance gain respectively. For comparisons, we choose MCD(Saito et al., 2017b) as a baseline since its assumption about the hypothesis space is similar to our SHS proposal. Besides, the two methods share the same network architecture in implementation, which makes the experimental results directly comparable. From Tab. 7, it can be seen that the 4th row of our method shows the effectiveness of the proposed upper bound, where we use L_1 as the discrepancy measurement without involving any pseudo target information and improve the performance compared to MCD in the 1st row. The 6th row shows the result when replacing it with the cross margin discrepancy. The last row shows the result when leveraging the information from pseudo-labeled target samples to construct a more reliable hypothesis space for f_2. These results show that every part of our proposal helps to improve the performance. In order to further verify the effectiveness of our proposal, we conduct another ablation study on VisDA dataset. The results in Tab. 8 reveal a similar conclusion that each part of our proposal is beneficial to the adaptation despite a more complicated scenario.

Table 8: A simple ablation study to reveal the contribution from each part of the proposal ($\surd$ in the column "optimal joint error" means to include the joint error in the upper bound, in contrast to the training objective proposed by MCD; $\surd$ in the column "cross margin discrepancy" means to use the proposed discrepancy measurement for ϵ, whereas $\times$ indicates we use L_1 norm instead; $\surd$ in the column "pseudo labels induced hypothesis space" means the hypothesis space for f_2 is built based on pseudo labels of target samples, which is corresponding to our THS proposal in the main paper where $\eta \neq 1$). We repeat the adaptation on VisDA dataset 3 times and report the average and the standard deviation of the accuracy.

METHOD	OPTIMAL JOINT ERROR	CROSS MARGIN DISCREPANCY	PSEUDO LABELS INDUCED HYPOTHESIS SPACE	VISDA
BASELINE	$\times$	$\times$	$\times$	71.9±0.4
	$\times$	$\surd$	$\times$	73.1±0.3
	$\times$	$\times$	$\surd$	76.2±0.3
	$\times$	$\surd$	$\surd$	76.8±0.2
OURS	$\surd$	$\times$	$\times$	73.4±0.3
	$\surd$	$\surd$	$\times$	76.4±0.3
	$\surd$	$\times$	$\surd$	79.2±0.2
	$\surd$	$\surd$	$\surd$	81.6±0.2